AD NUMBER
AD223952
CLASSIFICATION CHANGES
TO: **UNCLASSIFIED**
FROM: **CONFIDENTIAL**
LIMITATION CHANGES
TO: **Approved for public release; distribution is unlimited.**
FROM: **Distribution authorized to DoD only; Administrative/Operational Use; NOV 1961. Other requests shall be referred to Air Force Flight Test Center, Edwards AFB, CA.**
AUTHORITY
1 Jan 1964 per document markings; AFFTC ltr, 5 Aug 1969

CONFIDENTIAL

RESEARCH LABORATORIES

UNITED AIRCRAFT CORPORATION

UAC RESEARCH

CONFIDENTIAL

COPY NO. 62

UNITED AIRCRAFT CORPORATION
RESEARCH LABORATORIES

EAST HARTFORD, CONN.

Report R-2494-1

Theoretical Solutions for the
Secondary Flow on the End Wall of a
Vortex Tube

Contract AF 04(611)-7448

CONFIDENTIAL

REPORTED BY Olof L. Anderson
Olof L. Anderson

APPROVED BY Harlan D. Taylor
Harlan D. Taylor
Head, Aerophysics Section

NO. OF PAGES 75

DATE November 1961

FOREWORD

Contract AF 04(611)-7448 between the Air Force Flight Test Center, Edwards Air Force Base, California, Air Force Systems Command, United States Air Force and the Research Laboratories of United Aircraft Corporation pertains to investigations of the characteristics of a unique gaseous-core nuclear rocket concept. These investigations, which were directed toward the development of information pertinent to the evaluation of the feasibility of this concept, include the following: (1) experimental determination of the characteristics of vortex flow, (2) design and fabrication of equipment to provide a radial temperature gradient in a vortex flow, (3) theoretical calculations of the characteristics of the end-wall boundary layer in a vortex tube, and (4) theoretical calculations of radiant heat transfer in the proposed engine.

The work accomplished under the contract is summarized in the following Research Laboratories' reports which comprise the required Final Report:

I. Summary Report (Report R-2494-4)

II. Experimental Investigation of Characteristics of Confined Jet-Driven Vortex Flows (Report R-2494-2)

III. Heat Transfer to Confined Vortex Flows by Means of a Radio-Frequency Gas Discharge (Report R-2494-3)

IV. Theoretical Solutions for the Secondary Flow on the End Wall of a Vortex Tube (Report R-2494-1, Present Report)

V. Methods for Calculating Radiant Heat Transfer in High-Temperature Hydrogen Gas (Report M-1492-1)

Report R-2494-1

Theoretical Solutions for the Secondary Flow on the End Wall of a Vortex Tube

TABLE OF CONTENTS

Report R-294-1

Theoretical Solutions for the Secondary Flow on the End Wall of a Vortex Tube

Contract AF 04(611)-7448

SUMMARY

Theoretical solutions are presented for the growth of the tangential and radial components of both laminar and turbulent boundary layers in the secondary flow on the end wall of a vortex flow confined by a cylindrical tube having exit nozzles located on the axis of rotation at each of the two end walls. Solutions for a strong-vortex case (tangential velocity inversely proportional to radius) indicate that the weight flow entering the end-wall boundary layer is proportional to the friction between the tangential flow and the end wall. This weight flow is in many cases greater than the radial weight flow outside the end-wall boundary layer required to maintain a strong laminar vortex flow (greater by a factor of approximately 300 for a turbulent boundary layer, a tube length of 10 times the tube radius, and a Reynolds number based on tube radius and on the tangential velocity within the tube of 10^6). Solutions for the weak-vortex case in which the tangential velocities at small radii are less than that for the strong-vortex case are obtained by allowing for the reduction in vortex strength outside the end-wall boundary layer due to the loss of radial flow to the end-wall boundary layer. Solutions obtained for the weak-vortex case indicate that some of the weight flow entering the end-wall boundary layer near the outside radius of the tube will return to the main flow near the inside radius of the tube. The magnitude of the flow within the end-wall boundary layer offers a possible explanation of the weak-vortex strength which has been measured by several investigators and which had heretofore been attributed to turbulence within the primary flow outside the end-wall boundary layer.

All theoretical solutions obtained are based on assumed shapes for the tangential and radial boundary layer velocity profiles and assumed laws relating the tangential and radial wall friction to the Reynolds number of the flow. Sample calculations for the variation with radius of tangential velocity, boundary layer weight flow, and boundary layer thickness for a laminar boundary layer profile

and friction law are given for both the strong-vortex and the weak-vortex cases, whereas numerical examples for a turbulent boundary layer profile and friction law are given only for the strong-vortex case. The accuracy of results calculated from the theory should be limited only by the accuracy of the velocity profiles and shear formulas used in the calculation procedure.

The basic theoretical procedure and the sample calculations for laminar boundary layers were developed as part of the Research Laboratories' own research program. The adaptation of the theory to turbulent boundary layers and the calculation of the examples for turbulent boundary layers were made under Contract AF 04(611)-7448 with the Air Force Flight Test Center, Edwards Air Force Base, California, Air Force Systems Command, U. S. Air Force.

CONCLUSIONS

1. The radial mass flow in the boundary layers on the end walls of a cylindrical tube containing a vortex flow is proportional to the friction between the rotating flow and the end wall.

2. The passage of flow into the end-wall boundary layer is sufficient in many cases to cause a substantial reduction in the tangential velocities near the centerline of the vortex tube from those which would be obtained without an end-wall boundary layer. This calculated reduction in vortex strength due to secondary flow may explain the loss in vortex strength which has been measured by several investigators and which had heretofore been attributed to turbulence within the primary flow outside the end-wall boundary layer.

3. If the magnitude of the flow into the boundary layer is sufficient to cause a reduction of vortex strength, some of this boundary layer flow will return to the primary flow near the centerline of the vortex tube. In some cases the return of secondary flow to the primary flow region is sufficient to cause a radial outflow in the primary flow at certain radii within the vortex tube.

INTRODUCTION

Recently there has been a renewed interest in the use of vortex flows for applications in magnetohydrodynamic power generation (Ref. 1) and nuclear rocket propulsion (Ref. 2). The results of experimental studies of confined vortex flows, such as those described in Refs. 3, 4, and 5, indicate that these flows are considerably more complex than those generally assumed in one-dimensional analyses. It was suggested that vortex flows are turbulent and that certain three-dimensional phenomena, which are not well understood, might have a primary effect on such flows. Attempts at developing a satisfactory method for predicting the flow patterns obtained with a confined vortex were unsuccessful.

A further understanding of the characteristics of three-dimensional vortex flows was reported in Ref. 6. In particular, the existence of a two-cell vortex in an open-ended vortex tube was demonstrated. However, these results are not applicable to vortex flows confined by end walls. Another analysis, reported in Ref. 7, considered vortex flows in cylindrical tubes having end walls and included a friction factor to account for the end-wall boundary layer. However, because this analysis was also one-dimensional, the results cannot be used to predict any of the three-dimensional effects existing in vortex tubes.

Finally, subsequent to the completion of current studies on vortex flows at the UAC Research Laboratories, two papers on such flows (Refs. 8 and 9) were received which apply directly to the work reported herein. Reference 8 is an analytical study of the laminar boundary layer on a disc in a rotating flow with prescribed tangential velocity distributions. The analytical procedure is essentially that used in this report. However, because this analysis considered only the semi-infinite vortex, the complex interaction between the primary and secondary flows was not examined. Reference 9 is an experimental study of vortex flow which indicates that as much as 90% of the vortex mass flow may be carried in the end-wall boundary layer.

The object of the study reported herein was to formulate a three-dimensional theory for confined vortex flows in order to calculate the effects of the end-wall boundary layer and secondary axial flow on the distribution of angular momentum and tangential velocity in the primary flow of the vortex.

FLOW MODEL AND BASIC ASSUMPTIONS

A diagram of the analytical model used in the analysis is shown in Fig. 1. The vortex is assumed to be contained in a cylinder of radius r_1 and length z_1, and the flow is uniformly injected into the cylinder at r_1 with a tangential velocity $\bar{u}_{\phi_1}$, and a radial velocity $\bar{u}_{r_1}$. Two exit nozzles of radius r_* are located at each end of the vortex tube concentric with the axis of the cylinder.

A sketch showing the velocities considered in the analysis is given in Fig. 2. The secondary flow in the end-wall boundary layer is characterized by large radial velocities relative to the radial velocities in the primary flow. The origin of this radial flow can be understood from the following discussion. In the primary flow the centrifugal forces produced by the tangential motion of the fluid are balanced by the radial pressure gradient. However, in the end-wall boundary layer the tangential velocity is reduced to zero at the wall by shear forces, but the radial pressure gradient remains. This radial pressure gradient accelerates the flow in the boundary layer to large radial velocities relative to the radial velocities in the primary flow. Thus, although the boundary layer thickness is small, an appreciable fraction of the radial flow may pass through this end-wall boundary layer.

The following assumptions are employed in the analyses discussed in this report:

1. The flow is incompressible.
2. The flow is rotationally symmetric.
3. The pressure gradient in the axial direction in both the primary and secondary flows is zero.
4. The thickness of the boundary layer on the end walls is small relative to the radius of the vortex tube.
5. The thickness of the boundary layer in the tangential direction is equal to the thickness of the boundary layer in the radial direction.
6. Both the radial and tangential velocity profile shapes within the boundary layer are independent of radius.
7. The friction governing the shear between the flow within the boundary layer and the end wall of the tube is a function of the Reynolds number based on the thickness of the boundary layer in the end wall. (See Appendix A).

8. The flow outside the boundary layer is laminar (see discussion in section entitled Limit of Applicability of Strong-Vortex Solut on).

9. The radial velocity is much less than the tangential velocity in the primary flow outside the end-wall boundary layer.

10. The tangential velocity outside the end-wall boundary layer is independent of axial distance. This assumption is justified by the data presented in Refs. 1 and 10 and is proven analytically in Appendix A for the special case with the tangential velocity much larger than the radial velocity.

11. The radial velocity outside the end-wall boundary layer is independent of axial distance.

12. The axial velocity of the flow passing through the exit nozzles (see Fig. 1) is independent of radius within these nozzles.

GENERAL FORM OF SOLUTIONS

The general form of the solutions to be obtained can be shown by considering a torque balance at the end wall of a vortex tube. In this torque balance the moment created by the shear force between the moving fluid and the wall must be counteracted by a moment created by the change in tangential velocity of the flow entering the boundary layer.

$$w_s \bar{u}_{\phi_1} r_1 \sim \bar{C}_f (\pi r_1^2) \left(\frac{\rho \bar{u}_{\phi_1}^2}{2}\right) r_1 \qquad (1)$$

where w_s is mass flow entering boundary layer.

$\bar{u}_{\phi_1}$ is tangential velocity - proportional to change in tangential velocity of flow entering boundary layer.

r_1 is moment arm.

$\bar{C}_f$ is friction coefficient.

πr_1^2 is surface area of end wall of vortex tube.

$\frac{\rho u_{\phi_1}^2}{2}$ is dynamic pressure of rotating gas.

Therefore, the mass flow within the boundary layer on one end wall of a vortex tube is proportional to the right-hand side of the following equation.

$$W_s \sim \bar{C}_f \pi r_1^2 \rho \bar{u}_{\phi_1} \tag{2}$$

However, from the definition of tangential Reynolds number

$$Re_t = \frac{\rho \bar{u}_{\phi_1} r_1}{\mu} \tag{3}$$

$$W_s \sim \bar{C}_f (\pi r_1 \mu) Re_t \tag{4}$$

It is assumed that the friction coefficient varies with Reynolds number the same as on a flat plate. For laminar flow

$$\bar{C}_{f_L} \sim \frac{1}{Re_t^{1/2}} \tag{5}$$

Therefore,

$$W_{SL} = K_L (2\pi r_1 \mu) Re_t^{1/2} \tag{6}$$

The coefficient K_L in Eq. (6) must be chosen to account for all of the constants missing in the preceding equations.

For turbulent flow

$$\bar{C}_{f_T} \sim \frac{1}{Re_t^{1/5}} \tag{7}$$

Therefore,

$$W_{ST} = K_T (2\pi r_1 \mu) Re_t^{4/5} \tag{8}$$

It is also assumed that the expressions for the variation of boundary layer thickness with Reynolds number are similar to the corresponding expressions for flow over a flat plate.

$$\frac{\delta_L}{r_1} = \frac{\zeta_L}{Re_1^{1/2}} \tag{9}$$

$$\frac{\delta_T}{r_1} = \frac{\zeta_T}{Re_1^{1/5}} \tag{10}$$

The procedures employed to develop relations for the four coefficients, K_L, K_T, ζ_L, and ζ_T which are required to evaluate Eqs. (6), (8), (9), and (10) are developed in Appendixes A and B.

STRONG-VORTEX SOLUTION

The results discussed in the following section were obtained on the basis that the vortex is sufficiently strong that the angular momentum of the flow outside the boundary layer is constant (velocity outside the boundary layer inversely proportional to radius).

Specific Solutions for Strong-Vortex Case

A complete solution of the flow in the boundary layer on the end wall of the vortex tube requires consideration of the radial momentum equation as well as the tangential momentum equation employed in the preceding section. In this radial momentum equation, the radial acceleration of the flow within the boundary layer is determined by the forces resulting from the radial static pressure gradient, the radial shear on the end wall of the vortex tube, and the change in radial velocity of the mass flow entering the boundary layer from the primary flow outside the boundary layer. Procedures for simultaneous solution of the tangential and radial momentum equations are discussed in Appendix A.

To obtain a solution for the tangential and radial momentum equations, it is necessary to assume a shape for both the tangential and radial velocity profiles. Plots showing the tangential and radial velocity profiles which have been employed in the analyses are shown in Figs. 3 and 4. Two of the three profiles shown in

each of the figures are for laminar flow, whereas the third profile shape is for turbulent flow. Results of calculating the value of K_L at the exit radius for different combinations of laminar velocity profiles are shown in Table I. It can be seen from Table I that the value of K_{L*} (which is employed in calculating the weight flow in the boundary layer in Eq. (6) at $R = R_*$) varies by a factor of slightly more than two for the two extreme results. In an effort to choose the most likely laminar boundary layer profile to be encountered in a vortex tube, each of the profile combinations shown in Table I was used in an analysis of the secondary flow on a rotating disc (see Appendix B). The results of comparing the boundary layer mass flow calculations on a rotating disc with a known exact solution indicated that velocity profiles (1) and (12) in Figs. 3 and 4 would result in the best agreement with the exact solution. (The secondary mass flow on a rotating disc depends directly on the parameter B. Table II presents a comparison of the exact value of B with the approximate values given by the several assumed velocity profiles.) According to Table I, the value of K_{L*} for profiles (1) and (12) is

$$K_{L*} = 1.226 \tag{11}$$

Therefore the mass flow in the boundary layer on one end wall of a vortex tube at a value of R_* of 0.1 is, from Eq. (6),

$$W_{SL*} = 1.226\,(2\pi r_1 \mu)\,Re_1^{1/2} \tag{12}$$

The value of K_{T*} for turbulent flow for profiles (3) and (13) given in Figs. 3 and 4 is

$$K_{T*} = 0.113 \tag{13}$$

The corresponding expression for the mass flow in the boundary layer on one end wall of a vortex tube at a value of R_* of 0.1 is, from Eq. (8),

$$W_{ST*} = 0.113\,(2\pi r_1 \mu)\,Re_1^{4/5} \tag{14}$$

Curves determined from Eqs. (12) and (14) are given as a function of tangential Reynolds number in Fig. 5. As noted on the figure, the transition Reynolds number observed in tests of rotating discs is on the order of 10^5 (see Ref. 9).

A plot showing the variation with radius of the dimensionless radial mass flow within the boundary layer on one end wall of a vortex tube is given in Fig. 6 for both the laminar flow and turbulent flow solutions. The values given in Fig. 6 for a value of $R_* = 0.1$ correspond to the constants in Eqs. (11) through (14).

An analytical solution is given in Appendix A for the variation of boundary layer thickness with radius for a laminar boundary layer on the end wall of a vortex tube. The dimensionless boundary layer thickness for R between R_* and 1.0 from Eq. (122) of Appendix A is as follows:

$$\zeta_L = Re_1^{1/2} \frac{\delta_L}{r_1} = 0.931(-\sigma_1)^{1/4} R^{2/3}(1-R^{4/3})^{1/4} \qquad (15)$$

The constant $(-\sigma_1)^{1/4}$ in the preceding equation is presented in Table I for four different combinations of laminar velocity profiles. It can be seen from Table I that the variation of this constant among the different profiles is less than the variation of K_{L*} among the same profiles. The variation of ζ_L with radius for laminar profiles (1) and (12) in Figs. 3 and 4 is given in Fig. 7. The variation of ζ_L with radius for the different laminar profiles in Table I is identical. However, the absolute value of ζ_{L*} at any value of R_* is proportional to the value of the constant in Table I.

Also shown in Fig. 7 is the variation of ζ_T with radius for a turbulent boundary layer having profile shapes (3) and (13) of Figs. 3 and 4. The numerical solution used to obtain ζ_T for the turbulent layer is described in Appendix A.

Limit of Applicability of Strong-Vortex Solution

The strong-vortex solutions are valid as long as there is sufficient radial mass flow in the primary flow outside the end-wall boundary layer to provide the tangential momentum to overcome the shear forces which exist near the centerline of the vortex. This required radial mass flow is usually given in terms of the radial Reynolds number, Re_r, defined as follows:

$$Re_r = \frac{\rho \bar{u}_{r_1} r_1}{\mu} = \frac{W}{2\pi\mu z_1} \qquad (16)$$

The effect of radial Reynolds number on the variation of tangential velocity with radius for the case of zero secondary flow is given in Fig. 8. It can be seen from Fig. 8 that the vortex strength begins to fall off rapidly between a radial Reynolds number of 10 and 5. The criterion given in Fig. 8 does not hold when there is a substantial amount of flow within the end-wall boundary layer. For this case, an effective Reynolds number based on the flow outside the end-wall boundary layer must be employed. If σ is defined as the ratio of the flow within the boundary layer on both end walls of the vortex tube to the total flow passing through the vortex tube, then,

$$(Re_r)_{eff} = Re_r(1 - \sigma_*) \tag{17}$$

In the preceding equation σ_* is the value of σ at the exit radius where the greatest amount of flow has entered the boundary layer. From the definition of σ,

$$\sigma = \frac{2W_s}{2\pi r_1 z_1 \rho \bar{u}_{r_1}} \tag{18}$$

Substituting from Eq. (6), which gives the flow in the end-wall boundary layer with a laminar velocity profile,

$$\sigma_L = \frac{2K_L(\pi r_1 \mu) Re_f^{1/2}}{2\pi r_1 z_1 \rho \bar{u}_{r_1}} \tag{19}$$

From Eq. (16)

$$\sigma_L = 2K_L \frac{r_1}{z_1} \frac{Re_f^{1/2}}{Re_r} \tag{20}$$

Since

$$\frac{Re_f}{Re_r} = \frac{\bar{u}_{\phi_1}}{u_{r_1}} \tag{21}$$

Therefore,

$$\sigma_L = \frac{2K_L}{Re_t^{1/2}} \frac{r_1}{z_1} \frac{\bar{u}_{\phi_1}}{\bar{u}_{r_1}} \tag{22}$$

$$\sigma_L = K_L \left(\frac{2}{Re_t^{1/2}} \frac{\bar{u}_{\phi_1}}{\bar{u}_{r_1}} \frac{r_1}{z_1} \right) = K_L \beta_L \tag{23}$$

where the secondary flow parameter for laminar flow, β_L, is defined as follows:

$$\beta_L = \frac{2}{Re_t^{1/2}} \frac{\bar{u}_{\phi_1}}{\bar{u}_{r_1}} \frac{r_1}{z_1} \tag{24}$$

$$\beta_L = 2 \frac{r_1}{z_1} \frac{Re_t^{1/2}}{Re_r} \tag{25}$$

In the same manner, for turbulent flow,

$$\sigma_T = K_T \left(\frac{2r_1}{Z_1} \frac{Re_t^{4/5}}{Re_r} \right) \tag{26}$$

$$\sigma_T = K_T \beta_T \tag{27}$$

where the secondary flow parameter for turbulent flow, β_T, is given below.

$$\beta_T = \frac{2}{Re_t^{1/5}} \frac{\bar{u}_{\phi_1}}{\bar{u}_{r_1}} \frac{r_1}{z_1} \tag{28}$$

$$\beta_T = 2\frac{r_1}{z_1}\frac{Re_t^{4/5}}{Re_r} \tag{29}$$

Substituting Eqs. (23) and (27) into Eq. (17) yields

$$\beta_L = \frac{1}{K_L}\left[1 - \frac{(Re_r)_{eff}}{Re_r}\right] \tag{30}$$

$$\beta_T = \frac{1}{K_T}\left[1 - \frac{(Re_r)_{eff}}{Re_r}\right] \tag{31}$$

As noted in a preceding paragraph, an effective radial Reynolds number of between 5 and 10 is required to provide a strong vortex outside the end-wall boundary layers. Therefore, values of $(Re_r)_{eff}$ of 5 and 10 were used in evaluating Eqs. (30) and (31). The results of this evaluation are presented in Fig. 9. It can be seen from Fig. 9 that the maximum permissible value of the secondary flow parameter for applicability of the strong-vortex results increases with an increase in radial Reynolds number.

The limit of applicability for the strong-vortex results can also be presented in terms of tangential Reynolds number by combining Eqs. (30) and (31) with Eqs. (25) and (29). The results obtained in this manner using a value of $(Re_r)_{eff}$ of 5 are presented in Fig. 10 for three different values of z_1/r_1. The tangential Reynolds number must be lower than that shown in Fig. 10 if the strong-vortex results are to apply. The results presented in Figs. 9 and 10 were derived on the basis that the vortex strength was determined entirely by the radial mass flow at a radius equal to R_*. In practice, the tangential velocity profile is determined by some kind of average of the radial mass flows which exist outside the boundary layer at all values of radius. A more exact calculation of the limiting value of β_L for applicability of the laminar strong-vortex results will be described in a following section.

Data on vortex strength are presented in Refs. 3, 4, and 5 for radial Reynolds numbers ranging from 20 to 2000. According to Fig. 8 these radial Reynolds numbers should produce strong vortices if the fraction of the flow in the end-wall boundary layers is small and if the flow outside the end-wall boundary layers is laminar. However, the velocity profiles reported in Refs. 3 and 4 corresponded to radial Reynolds numbers on the order of 2 to 4. These differences between measured

Reynolds numbers based on total mass flow and Reynolds numbers determined from velocity profiles were attributed in Refs. 3 and 4 to turbulence outside the end-wall boundary layer. However, this same result could be obtained by the passage of a large percentage of the total radial mass flow through the end-wall boundary layers. To check this possibility, the results presented in Fig. 5 were employed to calculate the secondary flow for the data presented in Refs. 3, 4, and 5. The resulting calculated values of secondary flow were divided by the total measured mass flow in each test and the results are presented in Fig. 11 as a function of tangential Reynolds number. It can be seen from Fig. 11 that the calculated secondary flows are higher than the total mass flow in the vortex tubes for most of the test points. Therefore, it is possible that all of the loss in vortex strength reported in Refs. 3 and 4 is due to secondary flow rather than to turbulence. The significance of values of secondary flow calculated by the strong-vortex theory being greater than the total flow passing through the vortex tube will be discussed in the following section. The hypothesis of loss in vortex strength due to secondary flow is also strengthened by a measurement reported in Ref. 9 in which 90% of the total radial mass flow in a vortex tube was found to pass down the end-wall boundary layer. Insufficient data were reported in Ref. 9 to permit calculation of the theoretical weight flow corresponding to this measured weight flow.

WEAK-VORTEX SOLUTION

As noted in the preceding section, the strong-vortex solution is no longer valid when the mass flow passing into the end-wall boundary layer is so great that there is insufficient radial flow outside the boundary layer to maintain a strong vortex. The solution of the weak-vortex case requires simultaneous solution of the boundary layer and primary flow equations. The procedure employed is described in Appendix A. All calculations discussed in the following subsections were obtained on the basis of laminar flow in the boundary layers with profiles (1) and (12) in Figs. 3 and 4. However, the qualitative nature of the results is expected to apply for turbulent boundary layers.

Solutions for Fixed Radial Reynolds Number

A series of solutions was obtained for a fixed value of the radial Reynolds number of 10 and for a series of values of the secondary flow parameter, β_L. It can be seen from Eq. (25) that an increase in β_L for a fixed vortex tube geometry and a fixed value of radial Reynolds number represents an increase in tangential Reynolds number. The effect of an increase in β_L on the variation

of angular momentum and tangential velocity with radius is shown on Figs. 12 and 13. It can be seen from these figures that an increase in β_L and the accompanying increase in secondary flow (see Eqs. (17) and (23)) results in a decrease in vortex strength near the centerline of the vortex tube. The variation of static pressure coefficient with radius is shown in Fig. 14 for several values of β_L . Since the change of pressure with radius is directly proportional to the square of the tangential velocity, the differences in static pressure distributions shown in Fig. 14 for the different values of β_L are directly due to the decrease of vortex strength with increasing β_L . The curves in Figs. 13 and 14 for $\beta_L = 0$ are identical to those employed in the analyses in Refs. 3, 4, and 5.

The radial mass flow in the end-wall boundary layer is shown as a function of radius in Figs. 15 and 16 for different values of the secondary flow parameter, β_L . It can be seen from Fig. 15 that the nondimensional mass flow within the end-wall boundary layer at small values of radius decreases with an increase in β_L ; i.e., with a decrease in vortex strength near the centerline of the tube (see Figs. 12 and 13), although the fraction of secondary flow increases. It can also be seen from Figs. 15 and 16 that the radial mass flow in the end-wall boundary layer decreases with decreasing radius near the centerline of the vortex tube. The reason for this reversal of trend in the variation of boundary layer mass flow with radius is as follows. Near the outer radius of the tube there is more of a tendency to maintain constant angular momentum in the primary flow than in the secondary flow; therefore, flow passes from the primary to the secondary in an effort to maintain angular momentum in the secondary flow. However, at low values of radius the tendency to maintain angular momentum in the secondary flow is greater than in the primary flow; therefore, there is a tendency for flow to pass from the secondary flow to the primary flow in an effort to maintain a strong vortex in the primary flow. The significance of values of σ greater than unity in Fig. 16 is discussed in a following paragraph. The passage of flow from the boundary layer to the main stream is also predicted by the theory of Ref. 8 and some experimental verification is given by the ink-dye experiments reported in Ref. 9.

The variation of dimensionless boundary layer thickness with radius for several values of the secondary flow parameter, β_L , is shown in Fig. 17. It can be seen from Fig. 17 that an increase in β_L results in an increase in dimensionless boundary layer thickness even though it results in a decrease in mass flow within the boundary layer.

The streamlines formed by axial and radial velocities for a particular vortex tube geometry are plotted in Figs. 18 through 20 for values of the secondary flow parameter β_L of 0.4, 1.0 and 4.0 and for $Re_r = 10.0$. The

geometry of the vortex tube is defined by $R_* = 0.10$ and $z_1/r_1 = 6.0$. Since the vortex tube is symmetrical about the axis and the $z/z_1 = 1/2$ plane, the streamlines are plotted for only one quadrant. The tangential velocity distribution is also shown on these figures. Of particular interest are the streamlines in Fig. 20 which illustrate the "vortex cell" condition in which there is radial outflow in the primary flow. In order to preserve continuity, the inward flow in the end-wall boundary layer is equal to the sum of the outward flow in the vortex cell and the total mass flow passing through the vortex tube. This vortex cell condition arises when the secondary flow necessary to overcome friction on the end wall is greater than the flow injected into the vortex tube.

Effect of Radial Reynolds Number on Weak-Vortex Solution

The variation of angular momentum, tangential velocity, secondary mass flow, and boundary layer thickness with radius for several values of the secondary flow parameter, β_L, are presented in Figs. 21 through 24 for a radial Reynolds number of 5 and in Figs. 25 through 28 for a radial Reynolds number of 20. It can be seen by comparing Figs. 21 and 22 with Figs. 12 and 13 that a decrease in radial Reynolds number results in an increased sensitivity of tangential velocity profiles to the secondary flow parameter, β_L. The converse can be seen by comparing Figs. 25 and 26 with Figs. 12 and 13.

The ratios of secondary flow to total flow obtained from Figs. 16, 23, and 27 are summarized in Figs. 29 and 30. The maximum value of σ, denoted as σ_M, is presented in Fig. 29 whereas the value of σ at the nozzle exit radius, σ_*, is presented in Fig. 30. It can be seen from these figures that the secondary flow ratio decreases from that calculated for the strong-vortex solution as the secondary flow parameter is increased. The fraction of flow recirculated; i.e., the flow which is returned from the boundary layer to the primary flow divided by the total flow passing through the vortex, $\sigma_M - \sigma_*$, is presented in Fig. 31. These results were obtained from Figs. 29 and 30.

The preceding discussions indicate the existence of several flow regimes in a vortex tube. These flow regimes are shown in Fig. 32. Two separate criteria are used to separate the different flow regimes: one criterion describing the strength of the vortex (solid lines in Fig. 32), and the other criterion describing the fraction of the flow passing through the end-wall boundary layer (dashed lines in Fig. 32). The curve separating the strong-vortex regime from the weak-vortex regime is defined such that the tangential velocity at the exit radius is equal to 95% of the tangential velocity which would exist in an inviscid vortex. (This curve on Fig. 32 falls midway between the two curves for laminar flow given on Fig. 9.) The curve separating the weak-vortex regime from the very weak-vortex regime is defined such that the tangential velocity at the exit radius is equal to the tangential velocity at the outside radius of the vortex tube.

The secondary flow regimes are distinguished by the values of σ_M , the ratio of the maximum value of the flow in the end-wall boundary layers to the total flow passing through the vortex tube. The small secondary flow regime is defined such that σ_M is less than 0.1. The large secondary flow regime is defined where σ_M is between 0.1 and 1.0. Finally, the vortex cell regime is defined where σ_M is greater than 1 such that some of the fluid is trapped in a vortex cell, as shown by the streamline pattern in Fig. 20. It can be seen from Fig. 32 that there is a regime where there are large secondary flows and a strong vortex and also a regime where there are trapped vortex cells and a weak vortex motion.

REFERENCES

1. Donaldson, C. duP.: The Magnetohydrodynamic Vortex Power Generator, Basic Principles and Practical Problems. ARAP Report No. 30, 1961.

2. Kerrebrock, J. L. and R. V. Megreblian: An Analysis of Vortex Tubes for Combined Gas Phase Fission-Heating and Separation of the Fissionable Material. ORNL CF-57-11-3 Rev. 1, April 1958.

3. Keyes, J. J.: An Experimental Study of Gas Dynamics in High Velocity Vortex Flow. Proc. Heat Transfer and Fluid Mechanics Inst., Stanford University, June 1960.

4. Keyes, J. J., and R. E. Dial: An Experimental Study of Vortex Flow for Application to Gas-Phase Fission Heating. ORNL-2837, April 1960.

5. Ragsdale, R. G.: NASA Research on the Hydrodynamics of the Gaseous Vortex Reactor. NASA TN D-288, September 1960.

6. Donaldson, C. duP. and R. D. Sullivan: Behavior of Solutions of the Navier-Stokes Equations for a Complete Class of Three-Dimensional Viscous Vortices, Proc. Heat Trans. and Fluid Mech. Inst., Stanford University, June 1960.

7. Rietema, K., and H. J. Krajenbrink: Theoretical Derivation of Tangential Velocity Profiles in a Flat Vortex Chamber - Influence of Turbulence and Wall Friction. App. Sci. Res., Sec. A, Vol. 8, No. 223, 1959.

8. Mack, L.: Laminar Boundary Layer on a Disk in a Rotating Flow. JPL Research Summary No. 36-9, July 1, 1961.

9. Kendall, J.: Vortex Separation Experiments. JPL Research Summary No. 36-3, June 15, 1960.

10. Hartnett, J. P. and E. R. G. Eckert: Experimental Study of the Velocity and Temperature Distribution in a High Velocity Vortex Tube. Proc. Heat Transfer and Fluid Mech. Inst., 1956.

11. Schlichting, H.: Boundary Layer Theory. Pergamon Press, 1955.

12. Hall, M. S.: The Momentum Integral Equations for Three-Dimensional Laminar Boundary Layers in Incompressible Flow. Australian Aeronautical Research Committee Report ACA-62. November 1959.

LIST OF SYMBOLS

a_1, a_2	Numerical constants obtained from velocity profiles, Eqs. (88) and (89)
b	Constant, Eq. (96)
B	Proportionality constant for radial mass flow on rotating disc, Eq. (135)
c_1, c_2	Numerical constants, Eqs. (118) and (119)
$\bar{C}_f$	Effective skin-friction coefficient, Eq. (1)
C_p	Static pressure coefficient, $\frac{\bar{p} - \bar{p}_1}{1/2 \rho \bar{u}_{\phi_1}^2}$, Eq. (87)
f_1, f_2	Functions of radius only, Eq. (46)
F_1, F_2, F_3, F_4	Velocity distribution functions, Eqs. (76), (77), (137), and (138)
k_1, k_2, k_3, k_4, k_5	Numerical constants, Eqs. (113) to (117)
K_L, K_T	Proportionality constants for laminar and turbulent secondary flows, respectively
M_r	Radial momentum of secondary flow, lb
M_ϕ	Moment of momentum of secondary flow, ft-lb
p	Static pressure, lb/ft^2
$\bar{p}$	Static pressure in primary flow
P	Pressure force per unit radius acting on secondary flow, lb/ft
q	Dynamic pressure, $1/2 \rho \bar{u}_\phi^2$
Q	Radial mass flow for rotating disc, slugs/sec
r	Radius, ft
R	Dimensionless radius
Re_r	Radial Reynolds number, $\frac{\rho \bar{u}_{r_1} r_1}{\mu}$
$(Re_r)_{eff}$	Effective radial Reynolds number, Eq. (17)

LIST OF SYMBOLS (Cont.)

Re_t	Tangential Reynolds number, $\frac{\rho \bar{u}_{\phi_1} r_1}{\mu}$
Re_δ	Reynolds number based on boundary layer thickness, $\frac{\rho \bar{u}_{\phi_1} \delta}{\mu}$
T_ϕ	Torque per unit radius, lb
u_ϕ, u_r, u_z	Radial, tangential, axial velocities, ft/sec
$\bar{u}_\phi, \bar{u}_r, \bar{u}_z$	Radial, tangential, axial velocities in primary flow, ft/sec
U_R	Dimensionless radial velocity in primary flow, $\frac{\bar{u}_r}{\bar{u}_{r_1}}$
U_ϕ	Dimensionless tangential velocity in primary flow, $\frac{\bar{u}_\phi}{\bar{u}_{\phi_1}}$
$u_{z\,\delta}$	Axial velocity entering boundary layer
V_R	Average radial velocity in boundary layer, $\frac{W_S}{2\pi\rho r \bar{u}_{\phi_1}\delta}$, Eq. (78)
W_S	Secondary mass flow in one end-wall boundary layer, slugs/sec
z	Axial distance, ft
$\bar{z}$	Axial distance in boundary layer (dimensionless), z/δ
β_L	Secondary flow parameter (laminar), $\frac{2}{Re_t^{1/2}} \frac{\bar{u}_{\phi_1}}{\bar{u}_{r_1}} \frac{r_1}{z_1}$
β_T	Secondary flow parameter (turbulent), $\frac{2}{Re_t^{1/5}} \frac{\bar{u}_{\phi_1}}{\bar{u}_{r_1}} \frac{r_1}{z_1}$
δ	Boundary layer thickness
ϵ	Small quantity (dimensionless)
ζ_L, ζ_T	Dimensionless boundary layer thickness for a vortex tube (laminar - $Re_t^{1/2}\,\delta/r_1$)(turbulent - $Re_t^{1/5}\,\delta/r_1$)
η	Dimensionless boundary layer thickness for rotating disc ($Re_t^{1/2}\,\delta/r_1$)
λ	Dimensionless angular momentum, $\frac{r \bar{u}_{\phi_1}}{r_1 \bar{u}_{\phi_1}}$
μ	Molecular viscosity, lb sec/ft^2
ν	Kinematic viscosity, ft^2/sec

LIST OF SYMBOLS (Cont.)

ξ	Dummy variable of integration
ρ	Density, slugs/ft^3
σ	Secondary flow ratio, $\frac{2W_s}{2\pi r_1 \rho \bar{u}_{r_1} z_1}$
τ_r	Radial shear stress, lb/ft^2
τ_ϕ	Tangential shear stress, lb/ft^2
ψ	Stream function
Ψ	Dimensionless stream function, $\frac{\psi}{r_1 z_1 \bar{u}_{r_1}}$
ω	Angular velocity of rotating disc

Subscripts

1	Quantity evaluated at outer radius of vortex tube
*	Quantity evaluated at exit radius of vortex tube
L	Quantity evaluated for laminar boundary layers
M	Maximum value of quantity
T	Quantity evaluated for turbulent boundary layers

APPENDIX A

DERIVATION AND SOLUTION OF THE EQUATIONS DESCRIBING THE FLOW IN VORTEX TUBES

The equations of motion in cylindrical coordinates for a three-dimensional laminar vortex flow are

$$\frac{\partial (r u_r)}{\partial r} + \frac{\partial (r u_z)}{\partial z} = 0 \quad \text{Continuity} \tag{32}$$

$$u_r \frac{\partial u_r}{\partial r} + u_z \frac{\partial u_r}{\partial z} - \frac{u\phi^2}{r} = -\frac{1}{\rho}\frac{\partial p}{\partial r} + \nu \frac{\partial}{\partial r}\left[\frac{1}{r}\frac{\partial}{\partial r}(r u_r)\right] + \nu \frac{\partial^2 u_r}{\partial z^2} \tag{33}$$

Radial Momentum

$$\frac{u_r}{r}\frac{\partial (r u\phi)}{\partial r} + u_z \frac{\partial u\phi}{\partial z} = \nu \frac{\partial}{\partial r}\left[\frac{1}{r}\frac{\partial}{\partial r}(r u\phi)\right] + \nu \frac{\partial^2 u\phi}{\partial z^2} \tag{34}$$

Tangential Momentum

$$u_r \frac{\partial u_z}{\partial r} + u_z \frac{\partial u_z}{\partial z} = -\frac{1}{\rho}\frac{\partial p}{\partial z} + \nu \frac{1}{r}\frac{\partial}{\partial r}\left(r \frac{\partial u_z}{\partial r}\right) + \nu \frac{\partial^2 u_z}{\partial z^2} \tag{35}$$

Axial Momentum

Although the flow in vortex tubes is necessarily viscous everywhere, the flow in the main vortex (region of primary flow - see Fig. 1) may be considered separately from the thin viscous boundary layer in the end walls (region of secondary flow) for the purpose of deriving the governing equations of motion. This assumption is justified since the primary flow has well-defined and nearly constant properties in the axial direction and any strong axial gradients are, by definition, confined to the secondary flow region.

Primary Flow Region

The important properties and the governing equations of motion for the primary flow can be derived from Eqs. (32) through (35) by an order of magnitude

analysis. Assume, as is the case for most vortex flows, that the radial velocity is much smaller than the tangential velocity, i.e.,

$$\frac{\bar{u}_{r_1}}{\bar{u}_{\phi_1}} = O(\epsilon) \qquad \epsilon << 1 \tag{36}$$

Then, since the flow is injected into the vortex tube with constant mass flow per unit length, the order of magnitude of the derivatives in the z-direction are

$$\frac{\partial u_\phi}{\partial z} = O\left(\frac{\bar{u}_{\phi_1}}{z_1}\right) \quad ; \quad \frac{\partial u_r}{\partial z} = O\left(\frac{\bar{u}_{r_1}}{z_1}\right) \tag{37}$$

and the order of magnitude of the derivatives in the r-direction are

$$\frac{\partial u_\phi}{\partial r} = O\left(\frac{\bar{u}_{\phi_1}}{r_1}\right) \quad ; \quad \frac{\partial u_r}{\partial r} = O\left(\frac{\bar{u}_{r_1}}{r_1}\right) \tag{38}$$

With the use of Eq. (36), the zeroth order equations of motion for the primary flow are

$$\frac{\partial (r \bar{u}_r)}{\partial r} + \frac{\partial (r \bar{u}_z)}{\partial z} = 0 \qquad \text{Continuity} \tag{39}$$

$$\frac{1}{\rho} \frac{\partial \bar{p}}{\partial r} = \frac{\bar{u}_\phi^2}{r} \qquad \text{Radial Momentum} \tag{40}$$

$$\bar{u}_r \frac{1}{r} \frac{\partial (r \bar{u}_\phi)}{\partial r} + \bar{u}_z \frac{\partial \bar{u}_\phi}{\partial z} = \nu \frac{\partial}{\partial r}\left[\frac{1}{r} \frac{\partial}{\partial r}(r u_\phi)\right] + \nu \frac{\partial^2 u_\phi}{\partial z^2} \tag{41}$$

Tangential Momentum

$$\frac{\partial \bar{p}}{\partial z} = 0 \qquad \text{Axial Momentum} \tag{42}$$

Equations (40) and (42) state that the static pressure and tangential velocity are a function of r only and not a function of z. Consequently, the radial velocity is also a function only of r. This result has been verified experimentally in Ref. 10.

To satisfy Eqs. (39) through (42) the solution for the primary flow must have the following form:

$$\bar{u}_\phi = \bar{u}_\phi(r) \tag{43}$$

$$\bar{u}_r = \bar{u}_r(r) \tag{44}$$

$$\bar{p} = \bar{p}(r) \tag{45}$$

$$\bar{u}_z = f_1(r)\, z + f_2(r) \tag{46}$$

This class of solutions with an important generalization for a finite axial pressure gradient has been treated extensively in Ref. 6. By introducing Eqs. (43) through (46) into the conservation Eqs. (39) through (42) the governing equations reduce to

$$\frac{\partial(r\bar{u}_r)}{\partial r} = -r f_1(r) \tag{47}$$

$$\frac{1}{\rho}\frac{\partial \bar{p}}{\partial r} = \frac{\bar{u}_\phi^2}{r} \tag{48}$$

$$\frac{\bar{u}_r}{r}\frac{\partial}{\partial r}(r\bar{u}_\phi) = \nu\frac{\partial}{\partial r}\left[\frac{1}{r}\frac{\partial}{\partial r}(r\bar{u}_\phi)\right] \tag{49}$$

Laminar Secondary Flow Region, Including Primary Flow Interaction

The secondary flow, illustrated in Figs. 1 and 2, is associated with the flow in the boundary layers at the end walls of the vortex tube.

Since the conditions at the outer edge of these boundary layers are determined by the primary flow, which for the general case depends upon the amount of secondary flow, it is obvious that the two regions cannot be analyzed independently. Consequently, the derivation of the governing equations for the secondary flow included the interaction with the primary flow.

The equations governing the secondary flow were derived from Eqs. (32) through (35) by integrating over z between the limits $0 \le z \le z_1$. Two basic assumptions about the order of magnitude of terms in the differential equations were made.

$$\frac{\bar{u}_{r_1}}{\bar{u}_{\phi_1}} = O(\epsilon) \tag{50}$$

$$\frac{\delta}{r_1} = O(\epsilon) \tag{51}$$

From these two basic assumptions it is necessary to derive several auxiliary relations to simplify the equations. Let $\bar{u}_{\phi_1}$ be a typical tangential velocity in the boundary layer and u_r a typical radial velocity in the boundary with unspecified order of magnitude. Then in the boundary layer the order of magnitude of the derivatives are

$$\frac{\partial u_\phi}{\partial z} = O\left(\frac{\bar{u}_{\phi_1}}{\delta}\right) \quad ; \quad \frac{\partial u_r}{\partial z} = O\left(\frac{u_r}{\delta}\right) \tag{52}$$

$$\frac{\partial u_\phi}{\partial r} = O\left(\frac{\bar{u}_{\phi_1}}{r_1}\right) \quad ; \quad \frac{\partial u_r}{\partial r} = O\left(\frac{u_r}{r_1}\right) \tag{53}$$

By performing the order of magnitude analysis on Eqs.(32) through (35), the following results are obtained:

$$\left(\frac{u_z}{u_r}\,\frac{r_1}{\delta}\right) = O(1) \tag{54}$$

$$\left(\frac{\delta}{r_1}\sqrt{\frac{r_1\,u_r}{\nu}}\right) = O(1) \tag{55}$$

$$\frac{\partial p}{\partial z} = O(\epsilon^2)\left(\rho\frac{\bar{u}_{\phi_1}^2}{r_1}\right) \tag{56}$$

The last equation is significant because it proves that the axial pressure gradient in the end-wall boundary layer may be neglected in a zeroth order theory.

The order of magnitude of u_r must now be determined. From Eqs. (33), (56) and (40), it can be shown that,

$$\frac{1}{\rho}\frac{\partial p}{\partial r} = O\left(\nu\,\frac{u_r}{\delta^2}\right) = O\left(\frac{\bar{u}_{\phi_1}^2}{r_1}\right) \tag{57}$$

Then with the use of Eq. (55) one obtains the important result that

$$\frac{u_r}{\bar{u}_{\phi_1}} = O\ (1) \tag{58}$$

Finally, by substituting Eq. (58) into Eq. (55) one obtains the result that

$$\frac{\delta}{r_1} = O\left(\frac{1}{\sqrt{Re_1}}\right) = O\ (\epsilon) \tag{59}$$

The order of magnitude of the ratio of secondary to total flow is given by the parameter

$$\beta_L = 2\,\frac{2\pi r_1 \rho u_r \delta}{2\pi r_1 \rho \bar{u}_{r_1} z_1} = \frac{2}{\sqrt{Re_t}}\,\frac{\bar{u}_{\phi_1}}{\bar{u}_{r_1}}\,\frac{r_1}{z_1} \tag{60}$$

With these results, if terms of first order or higher in ϵ are neglected and if Eqs. (47) through (49) are used to describe the primary flow, then the governing equations reduce to

$$r\,\bar{u}_r\,z_1 + 2\int_0^\delta r\,u_r\,dz = -r_1\,\bar{u}_{r_1}\,z_1 \tag{61}$$

Continuity

$$\int_0^\delta \left[u_r\,\frac{\partial u_r}{\partial r} + u_z\,\frac{\partial u_r}{\partial z} - \frac{u_\phi^2}{r} + \frac{1}{\rho}\,\frac{\partial p}{\partial r} - \nu\,\frac{\partial^2 u_r}{\partial z^2}\right] dz = 0 \tag{62}$$

Radial Momentum

$$\int_0^\delta \left[\frac{u_r}{r}\,\frac{\partial (r\,u_\phi)}{\partial r} + u_z\,\frac{\partial u_\phi}{\partial z} - \nu\,\frac{\partial^2 u_\phi}{\partial z^2}\right] dz = 0 \tag{63}$$

Tangential Momentum

$$\frac{\partial p}{\partial z} = 0 \tag{64}$$

Axial Momentum

For convenience it is also determined that

$$(r\,u_z)_{z=\delta} = -\int_0^\delta \frac{\partial (r\,u_r)}{\partial r}\,dz \tag{65}$$

By carrying out the indicated integration in Eqs. (62) and (63) two integral boundary layer equations are obtained.

$$\frac{d}{dr}\int_0^{\delta}(ru_r)(ru_\phi)\,dz - r\bar{u}_\phi\frac{d}{dr}\int_0^{\delta}(ru_r)\,dz = -\nu r^2\left(\frac{\partial u_\phi}{\partial z}\right)_{z=0} \tag{66}$$

$$\frac{d}{dr}\int_0^{\delta} ru_r^2\,dz + \int_0^{\delta}(\bar{u}_\phi^2 - u_\phi^2)\,dz = -\nu r\left(\frac{\partial u_r}{\partial z}\right)_{z=0} \tag{67}$$

The following integral quantities are defined

$$M_\phi = 2\pi\rho\int_0^{\delta} r u_r\, ru_\phi\, dz \tag{68}$$

Moment of Momentum

$$W_s = 2\pi\rho\int_0^{\delta} ru_r\,dz \tag{69}$$

Secondary Mass Flow

$$T_\phi = 2\pi\rho\nu r^2\left(\frac{\partial u_\phi}{\partial z}\right)_{z=0} \tag{70}$$

Torque Per Unit Radius

$$M_r = 2\pi\rho\int_0^{\delta} ru_r^2\,dz \tag{71}$$

Radial Momentum

$$P = 2\pi\rho\int_0^{\delta}(\bar{u}_\phi^2 - u_\phi^2)\,dz \tag{72}$$

Pressure Force Per Unit Radius

$$r\tau_r = 2\pi\rho\nu r\left(\frac{\partial u_r}{\partial z}\right)_{z=0} \tag{73}$$

Shear Force Per Unit Radius

In terms of these newly defined quantities the integral equations (57) and (58) become

$$\frac{d M_r}{d r} - P = - r \tau_r \qquad (74)$$

Radial Momentum Equation

$$\frac{dM_\phi}{dr} - r \bar{u}_\phi \frac{dW_s}{dr} = - T_\phi \qquad (75)$$

Tangential Momentum Equation

Equation (74) states that the rate of change of radial momentum is equal to the difference between the pressure force and the radial shear force. Equation (75) states that the rate of change of moment of momentum is equal to the difference between the moment of momentum brought in from the primary flow and the torque exerted by the end walls. These equations are equivalent to the generalized three-dimensional boundary layer equations derived in Ref. 12.

The two integral boundary layer equations, Eqs. (74) and (75), contain six unknowns defined by Eqs. (68) through (73). Therefore, the problem now becomes one of writing four additional relations among the six unknowns. Unfortunately, experimental data or similarity solutions are not available and therefore it is not possible at this time to obtain the necessary relations in a completely satisfactory manner. In view of these difficulties, the following one-parameter families of velocity profiles are assumed for the tangential and radial velocity in the boundary layer.

$$u_\phi = \bar{u}_\phi F_1 \left(\frac{z}{\delta}\right) \qquad (76)$$

$$u_r = - \bar{u}_{\phi_1} V_R F_2 \left(\frac{z}{\delta}\right) \qquad (77)$$

where V_R is defined as the average velocity in the boundary layer by the relation

$$\bar{u}_{\phi_1} V_R \equiv -\frac{1}{\delta}\int_0^{\delta} u_r \, dz \tag{78}$$

Finally it is noted that for laminar flow, one boundary layer equation can be eliminated, if it is assumed that the average velocity is related to the Karmen-Pohlhausen parameter (see Ref. 12).

$$\bar{u}_{\phi_1} V_R = \frac{\bar{u}_\phi^2}{\nu r}\,\delta^2 \tag{79}$$

By substituting Eqs. (76) and (77) into Eqs. (68), (69), and (70), the following relations are obtained.

$$M_\phi = -2\pi\rho\left(\frac{\bar{u}_\phi^2}{\nu}\,\delta^2\right) r\,\bar{u}_\phi\,\delta\int_0^1 F_1 F_2\, d\bar{z} \tag{80}$$

$$W_{SL} = -2\pi\rho\left(\frac{\bar{u}_\phi^2}{\nu}\,\delta^2\right)\delta\int_0^1 F_2\, d\bar{z} \tag{81}$$

$$T_\phi = 2\pi\rho\nu r^2\,\frac{\bar{u}_\phi}{\delta}\,F_1'(0) \tag{82}$$

Substituting these three equations into the secondary flow tangential momentum equation, Eq. (66), and nondimensionalizing the term yields

$$\frac{d}{dR}\left[(RU_\phi)^3\,\frac{\zeta^3}{R^2}\right]\int_0^1 F_2 F_1\, d\bar{z} - RU_\phi\,\frac{d}{dR}\left[(RU_\phi)^2\,\frac{\zeta^3}{R^2}\right]\int_0^1 F_2\, d\bar{z} - \frac{R}{\zeta}\,RU_\phi F_1'(0) = 0 \tag{83}$$

Similarly, after nondimensionalizing the radial momentum and tangential momentum equations (Eqs. (48) and (49)) for the primary flow and the continuity equation (Eq. (61)) and using an integrating factor for Eq. (83) the following set of equations is obtained.

$$\frac{d^2\lambda}{dR^2} = \left[\frac{1}{R} + RU_R\right]\frac{d\lambda}{dR} \tag{84}$$

$$U_R = -\frac{1}{R} + \beta_L \lambda^2 \left(\frac{\zeta}{R}\right)^3 \int_0^1 F_2 \, d\bar{z} \tag{85}$$

$$\zeta_L = \left\{ a_1 \lambda^{-2a_2} R \int_0^R \lambda^{2(a_2-1)} \xi^{1/3} \, d\xi \right\}^{1/4} \tag{86}$$

In addition, the equation for the static pressure coefficient may also be written

$$C_p = \frac{\bar{p} - \bar{p}_1}{\frac{1}{2}\rho \bar{u}_{\phi_1}^2} = 2 \left[\int_0^R \frac{\lambda^2}{\xi^3} \, d\xi - \int_0^1 \frac{\lambda^2}{\xi^3} \, d\xi \right] \tag{87}$$

where

$$a_1 = \frac{F_1'(0)}{\frac{3}{4} \int_0^1 (F_3 F_1 - F_3) \, d\bar{z}} \tag{88}$$

$$a_2 = \frac{\int_0^1 (\frac{3}{2} F_3 F_1 - F_3) \, d\bar{z}}{\frac{3}{4} \int_0^1 (F_3 F_1 - F_3) \, d\bar{z}} \tag{89}$$

$$\beta_L = \frac{2}{\sqrt{Re_t}} \frac{\bar{u}_{\phi_1}}{\bar{u}_{r_1}} \frac{r_1}{z_1} \tag{90}$$

The parameter β_L is called the secondary flow parameter and is a measure of the fraction of the total flow which passes through the boundary layer. When $\beta_L = O(1)$ a significant fraction of the total flow moves radially inward through the end-wall boundary layer.

The velocity distribution functions F_1 and F_2 were chosen as simple polynomials by the procedure presented in Appendix B and satisfy the following conditions:

$$\begin{aligned} \bar{z} = 0 \qquad & F_1 = 0 \qquad & F_2 = 0 \\ & F_1'' = 0 \qquad & F_2'' = 1 \end{aligned} \tag{91}$$

$$\begin{aligned} \bar{z} = 1 \qquad & F_1 = 1 \qquad & F_2 = 0 \\ & F_1' = 0 \qquad & F_2' = 0 \\ & F_1'' = 0 \qquad & F_2'' = 0 \end{aligned} \tag{92}$$

The axial velocities and streamlines may be obtained from Eqs. (61) and (65). The stream function is

$$\Psi = \frac{\psi}{r_1 z_1 \bar{u}_{r_1}} = R U_R \left(\frac{z}{z_1} - \frac{1}{2} \right) - \frac{1}{2} \tag{93}$$

and the equation for the streamlines is

$$\frac{z}{z_1} = \frac{\psi + 1/2}{R U_R} + \frac{1}{2} \tag{94}$$

The coefficient, K_L, used in the strong-vortex solution is given by

$$K_L = \frac{\lambda^2}{R^2} \zeta^3 \int_0^1 F_2 \, d\bar{z} \tag{95}$$

Viscous Core Region

In the viscous core region (see Fig. 1) the end-wall boundary layer does not exist and the equations describing the flow are identical with those for the primary flow (Eqs. (47), (48), and (49)). The general form of the solutions is given by Eq. (46) with

$$f_1(r) = \frac{2b}{z_1} \quad ; \quad f_2(r) = -b \qquad 0 \le r \le r_* \tag{96}$$

When this solution is inserted into the continuity equation (Eq. (47)) and the result matched with the solution for the primary flow the following relationship is obtained:

$$RU_R = (RU_R)_* \frac{R^2}{R_*^2} \tag{97}$$

Substitution of Eq. (97) into the tangential momentum equation (Eq. (84)) yields

$$\lambda = \lambda_* \frac{\left[\exp\left(\frac{Re_r U_{R*}}{R_*}\frac{R^2}{2}\right) - 1\right]}{\left[\exp\left(\frac{Re_r U_R R_*}{2}\right) - 1\right]} \qquad 0 < R < R_* \tag{98}$$

Thus, the solution for the viscous core is given by Eqs. (97) and (98), provided values of λ_* and U_{R*} are known from the solution for the primary and secondary flow.

Turbulent Secondary Flow Region

When the primary flow vortex is sufficiently strong, the angular momentum outside the boundary layer is constant (strong-vortex case) and the secondary flow may be analyzed separately from the primary flow and the viscous core. For this case, the value of λ is 1 and a considerable simplification of the conservation equations makes it possible to also treat the case of turbulent flow in the end-wall boundary layer.

The turbulent velocity distribution is chosen to be

$$u_\phi = \bar{u}_\phi \, F_1 \left(\frac{z}{\delta}\right) \tag{99}$$

$$u_r = -\bar{u}_{\phi_1} V_R \, F_2\left(\frac{z}{\delta}\right) \tag{100}$$

Equations (99) and (100) may be substituted into Eqs. (68), (69), (70) and (72) to obtain

$$M_\phi = 2\pi\rho r^2 \bar{u}_\phi V_R \bar{u}_{\phi_1} \delta \int_0^1 F_2 F_1 \, d\left(\frac{z}{\delta}\right) \tag{101}$$

$$W_s = 2\pi\rho r_1 \bar{u}_{\phi_1} V_R \delta \int_0^1 F_2 \, d\left(\frac{z}{\delta}\right) = K_T 2\pi r_1 \mu \sqrt{Re_t} \tag{102}$$

$$M_r = 2\pi\rho r_1 \bar{u}_{\phi_1}^2 V_R^2 \delta \int_0^1 F_2^2 \, d\left(\frac{z}{\delta}\right) \tag{103}$$

$$P = 2\pi\rho \bar{u}_{\phi_1}^2 \delta \int_0^1 (1 - F_1^2) \, d\frac{z}{\delta} \tag{104}$$

Finally, in the absence of better information on turbulent end-wall boundary layer profiles, the shear stress equations are assumed to have the same form as for a flat plate.

$$\tau_\phi = \frac{.0225 \, \bar{u}_\phi^2}{\left(\frac{\delta \bar{u}_\phi}{\nu}\right)^{1/4}} \tag{105}$$

$$\tau_r = \frac{.0225\, u_{r_M}^2}{\left(\frac{\delta_M u_{r_M}}{\nu}\right)^{1/4}} \tag{106}$$

The velocity U_{r_M} is the maximum radial velocity in the boundary layer and δ_M is the axial distance at which it occurs. Substitution of Eq. (105) into Eq. (70) and Eq. (106) into Eq. (73) yields

$$T_\phi = 2\pi\rho r^2 \frac{.0225\, \bar{u}_\phi^2}{\left(\frac{\delta \bar{u}_\phi}{\nu}\right)^{1/4}} \tag{107}$$

$$r\tau_r = 2\pi\rho r \frac{.0225\, u_{r_M}^2}{\left(\frac{\delta_M u_{r_M}}{\nu}\right)^{1/4}} \tag{108}$$

Then, substitution of Eqs. (101) through (104), (107), and (108) into the radial and tangential momentum equations (Eqs. (74) and (75)) give

$$k_3 \frac{d}{dR}\left(R V_R^2 \zeta_T\right) = k_4 \frac{R V_R^2}{(\zeta_T V_R)^{1/4}} - k_2 \frac{\zeta_T}{R^2} \tag{109}$$

$$k_5 \frac{d}{dR}\left(R V_R \zeta_T\right) = .0225 \left(\frac{R}{\zeta_T}\right)^{1/4} \tag{110}$$

where

$$\frac{\sigma}{\beta_T} = k_1 R V_R \zeta_T \tag{111}$$

$$\zeta_T = Re_1^{1/5} \frac{\delta}{r_1} \tag{112}$$

$$k_1 = \int_0^1 F_2 \, d\left(\frac{z}{\delta}\right) \tag{113}$$

$$k_2 = \int_0^1 (1 - F_1^2) \, d\left(\frac{z}{\delta}\right) \tag{114}$$

$$k_3 = \int_0^1 F_2^2 \, d\left(\frac{z}{\delta}\right) \tag{115}$$

$$k_4 = \frac{.0225 \, C_2^2}{(C_1 C_2)^{1/4}} \tag{116}$$

$$k_5 = \int_0^1 F_2 (F_1 - 1) \, d\left(\frac{z}{\delta}\right) \tag{117}$$

$$C_1 = \left(\frac{z}{\delta}\right)_M \tag{118}$$

$$C_2 = F_2\left[\left(\frac{z}{\delta}\right)_M\right] \tag{119}$$

Equations (109) and (110) with auxiliary Eqs. (111) through (119) are the required equations for solution of the secondary flow in the turbulent end-wall boundary layer.

The coefficient $K_T(R)$ used in the solution of the strong-vortex case is given by

$$K_T = V_R \zeta \int_0^1 F_2 \, d\bar{z} \tag{120}$$

Boundary Conditions and Method of Solution

If Eq. (86) is substituted into Eq. (85) and Eq. (85) is substituted into Eq. (84), a single second-order differential equation in λ results. The solution is obtained by numerical integration with the boundary conditions.

$$R = 1.0 \qquad \lambda = 1.0 \qquad \zeta_T = 0 \tag{121}$$

$$R = R_* \qquad \frac{d\lambda}{dR} = \lambda_* Re_r U_{R_*} \frac{\exp\left(\frac{Re_r U_{R_*} R_*}{2}\right)}{\exp\left(\frac{Re_r U_{R_*} R_*}{2}\right) - 1} \tag{122}$$

The numerical solution for the strong-vortex case was obtained by setting $\beta_L = 0$, $Re_r = 1000$. These conditions were sufficient to maintain

$$\lambda = 1.0 \qquad 1.0 > R > R_* \tag{123}$$

Furthermore an analytical solution for the strong-vortex case may be obtained by substituting Eq. (123) into Eq. (86). The result is

$$\zeta_L = \sqrt{Re_f}\,\frac{\delta}{r_i} = \left(-\frac{3}{4}\,a_1\right)^{1/4} R^{2/3} (1-R^{4/3})^{1/4} \tag{124}$$

Equation (124) is very useful in comparing the effect of different assumed velocity profile shapes on the solution.

APPENDIX B

SELECTION OF THE BOUNDARY LAYER VELOCITY DISTRIBUTION FUNCTIONS

Laminar Boundary Layer

The equations describing the viscous flow adjacent to a rotating disc have been solved exactly (Ref. 10). As a means of selecting suitable velocity profiles for use in the vortex analysis, the radial mass flow on a rotating disc was evaluated using simple polynomial expressions for the velocity profiles. Comparison of the approximate mass flow computed using the assumed profiles with the exact mass flow indicated which of the assumed profiles gave the most accurate mass flow rates.

The momentum integral equation, Eq. (66), written in a form applicable to the rotating disc problem becomes

$$\frac{d}{dR}\int_0^{\delta}(ru_r)(ru_\phi)dz = -\nu r^2\left(\frac{\partial u_\phi}{\partial z}\right)_{z=0} \tag{125}$$

since

$$u_r(0) = 0 \tag{126}$$

$$u_\phi(\delta) = 0 \tag{127}$$

The tangential velocity distribution at the surface of the rotating disc is given by

$$u_\phi(0) = \omega r \tag{128}$$

The velocities are given by

$$u_\phi = r\omega F_3\left(\frac{z}{\delta}\right) \tag{129}$$

$$u_r = \frac{r\omega^2}{\nu}\,\delta^2 F_4\left(\frac{z}{\delta}\right) \tag{130}$$

Then substitution of Eqs. (128), (129), and (130) into Eq. (125) yields, after some mathematical manipulation, the equation

$$\frac{d}{dR}(\eta^3 r^4) = \frac{r^2}{\eta}\,\frac{F_3'(0)}{\int_0^1 F_3 F_4\, d\left(\frac{z}{\delta}\right)} \tag{131}$$

where

$$\eta = \sqrt{\frac{\omega}{\nu}}\,\delta \tag{132}$$

Since η is a constant for laminar flow, integration of Eq. (131) gives the nondimensional boundary layer thickness

$$\eta = \left[\frac{1}{4}\,\frac{F_3'(0)}{\int_0^1 F_3 F_4\, d\bar{z}}\right] \tag{133}$$

The induced radial mass flow at r is

$$Q = 2\pi r\int_0^\delta u_r\, dz = -2\pi r^2\sqrt{\nu\omega}\;\eta^3\int_0^1 F_4\, d\bar{z} \tag{134}$$

Define a quantity, B , by the relation

$$B = -2\eta^3\int_0^1 F_4\, d\bar{z} \tag{135}$$

Hence the radial mass flow becomes

$$Q = B\pi r^2\sqrt{\nu\omega} \tag{136}$$

The velocity distribution functions, F_3 and F_4, may be redefined in terms of the velocity distribution functions, F_1 and F_2, employed in the secondary flow analysis by the relations

$$F_3 = 1 - F_1 \tag{137}$$

$$F_4 = -F_2 \tag{138}$$

The constant, B, which depends on the velocity profiles, is given in Table II for comparison with the exact solution. It may be seen from the results presented in this table that velocity profiles (1) and (12) yield the best agreement with the exact value of B and, consequently, the exact secondary mass flow rate. Therefore, the following velocity distribution functions have been employed in evaluating the characteristics of a vortex tube with laminar flow in the end-wall boundary layer.

$$F_1 = 2\bar{z} - \bar{z}^2 \tag{139}$$

$$F_2 = 12(\bar{z} - 2\bar{z}^2 + \bar{z}^3) \tag{140}$$

Turbulent Boundary Layer

Since a simple 1/7-power law under most conditions describes flat-plate boundary layers, it has been chosen for the tangential velocity profile. For

the radial velocity profile, the 1/7-power law was also chosen with the addition of a polynomial needed to satisfy Eq. (81).

$$F_1 = \left(\frac{z}{\delta}\right)^{1/7} \tag{141}$$

$$F_2 = \left[\left(\frac{z}{\delta}\right)^{1/7} - \frac{13}{7}\left(\frac{z}{\delta}\right) + \frac{6}{7}\left(\frac{z}{\delta}\right)^2\right]\frac{56}{13} \tag{142}$$

These distribution functions are illustrated in Figs. 3 and 4.

TABLE I

Numerical Constants Evaluated for Several Combinations of Radial and Tangential Laminar Velocity Profiles

Tangential Velocity Profile (See Fig. 3)	Radial Velocity Profile (See Fig. 4)	Slope of Tangential Velocity Profile at Wall, $\frac{du_\phi}{d\bar{z}}\Big_{\bar{z}=0}$	Integral Required in Evaluating Eq. (77), $\int F_2 F_1 \, d\bar{z}$	Constant Proportional to Boundary Layer Mass Flow at $R_* = 0.1$ (See Eq. (6)) K_{L*}	Constant Proportional to Boundary Layer Thickness (See Eq. (124)) $(-a_1)^{1/4}$	Constant Employed in Evaluating Eq. (86) (See Appendix) a_2
(1) $2\bar{z} - \bar{z}^2$	(11) $6(\bar{z} - \bar{z}^2)$	2	$\frac{7}{10}$	2.145	3.22	$-\frac{2}{9}$
	(12) $12(\bar{z} - 2\bar{z}^2 + \bar{z}^3)$	2	$\frac{3}{5}$	1.226	4.23	$\frac{1}{3}$
(2) $\frac{3}{2}\bar{z} - \frac{1}{2}\bar{z}^3$	(11) $6(\bar{z} - \bar{z}^2)$	$\frac{3}{2}$	$\frac{13}{20}$	1.535	2.88	$\frac{2}{3}$
	(12) $12(\bar{z} - 2\bar{z} + \bar{z}^3)$	$\frac{3}{2}$	$\frac{19}{42}$	0.895	3.81	$\frac{13}{24}$

CONFIDENTIAL

TABLE II

Numerical Constants for Different Velocity Profiles for the Rotating Disc Boundary Layer

Tangential Velocity Profile (See Fig. 2)	Radial Velocity Profile (See Fig. 4)	Scope of Tangential Velocity Profile at the Wall $\left(\frac{du_\phi}{d\bar{z}}\right)_{\bar{z}=0}$	Integral Required in Evaluating Eq. (133) $\int F_3 F_4 \, d\bar{z}$	Constant Proportional to Boundary Layer Mass Flow at $R_* = 0.1$ (See Eq. (134)) B
$1-(2\bar{z}-\bar{z}^2)$	$-6(\bar{z}-\bar{z}^2)$	-2	$-\frac{3}{10}$	1.571
	$-12(\bar{z}-2\bar{z}^2+\bar{z}^3)$	-2	$-\frac{2}{5}$	0.897
$1-\left(\frac{3}{2}\bar{z}-\frac{1}{2}\bar{z}^3\right)$	$-6(\bar{z}-\bar{z}^2)$	$-\frac{3}{2}$	$-\frac{21}{60}$	1.065
	$-12(\bar{z}-2\bar{z}^2+\bar{z}^3)$	$-\frac{3}{2}$	$-\frac{48}{105}$	0.655
Exact Solution, Ref. 9				0.886

VORTEX TUBE GEOMETRY ASSUMED IN ANALYSIS

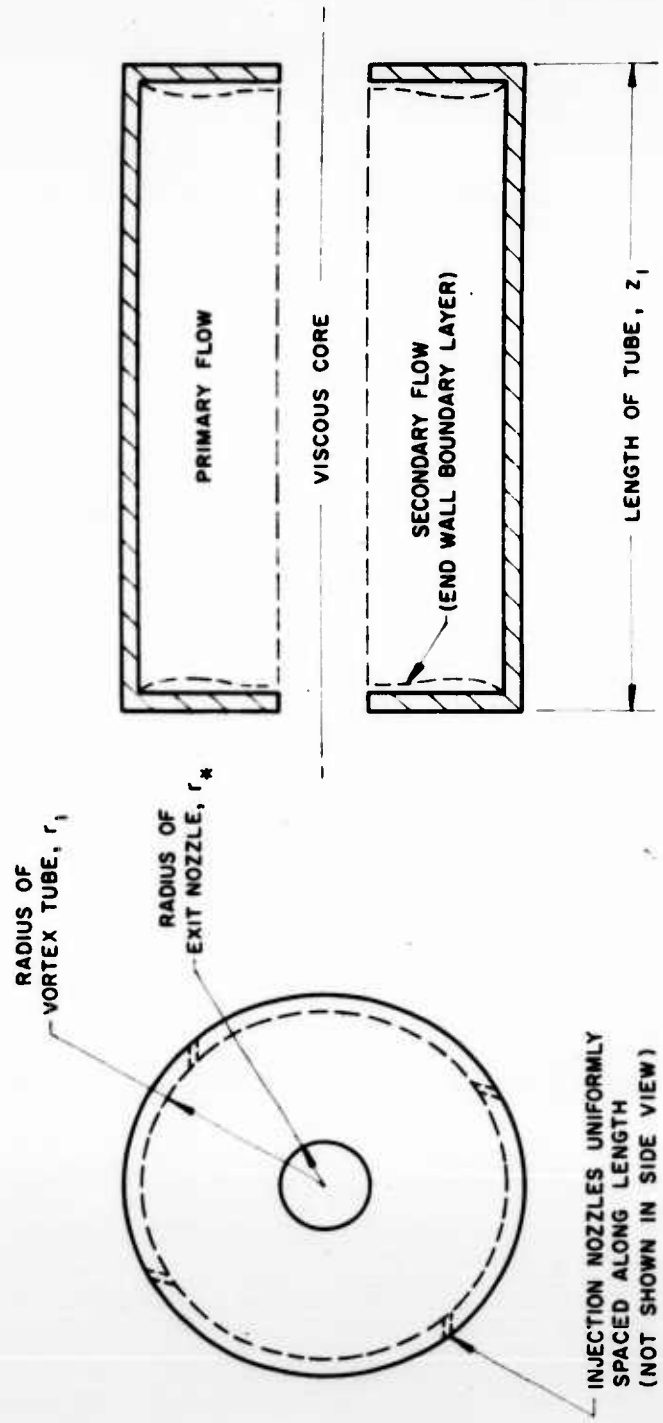

VELOCITIES CONSIDERED IN ANALYSIS

NOTE: $\bar{u}_{\phi_1}$ AND $\bar{u}_{r_1}$ ARE VALUES OF $\bar{u}_\phi$ AND $\bar{u}_r$ AT $r = r_1$

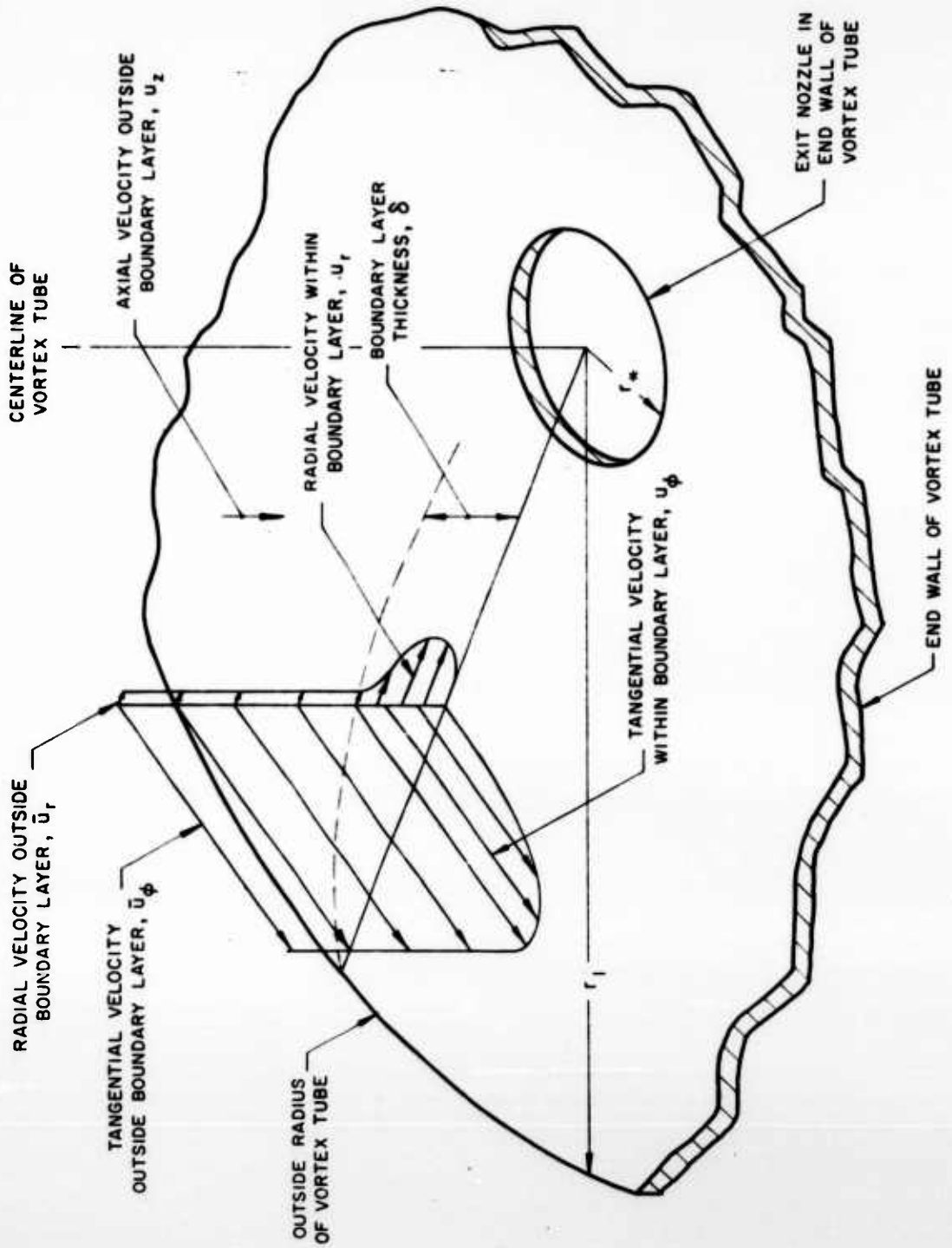

CONFIDENTIAL

FIG. 3

TANGENTIAL VELOCITY PROFILES CONSIDERED IN ANALYSIS

LAMINAR PROFILES

① $F_1 = 2\bar{z} - \bar{z}^2$

② $F_1 = \frac{3}{2}\bar{z} - \frac{1}{2}\bar{z}^3$

TURBULENT PROFILE

③ $F_1 = \bar{z}^{1/7}$

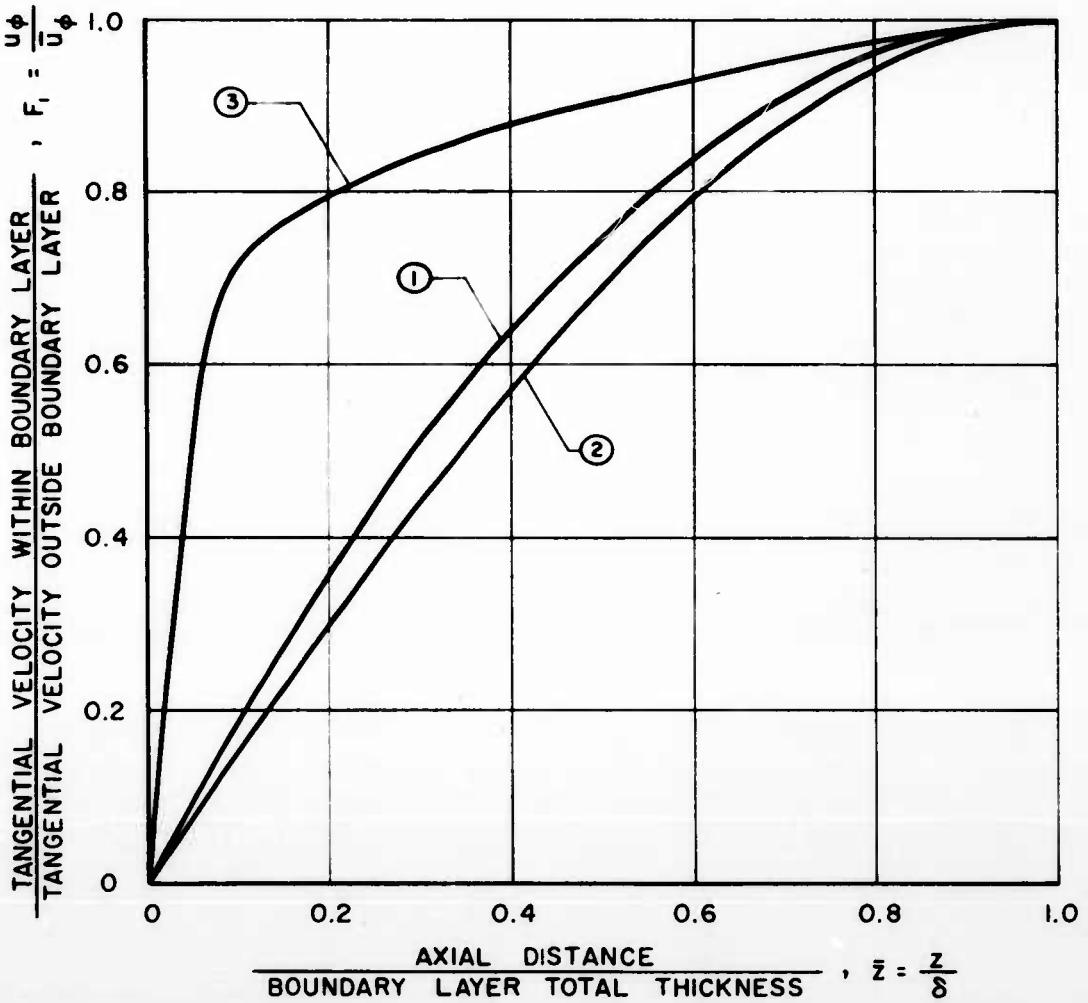

CONFIDENTIAL

CONFIDENTIAL

FIG. 4

RADIAL VELOCITY PROFILES CONSIDERED IN ANALYSIS

LAMINAR PROFILES

⑪ $F_2 = 6(\bar{z} - \bar{z}^2)$

⑫ $F_2 = 12(\bar{z} - 2\bar{z}^2 + \bar{z}^3)$

TURBULENT PROFILE

⑬ $F_2 = \frac{56}{13}(\bar{z}^{1/7} - \frac{13}{7}\bar{z} + \frac{6}{7}\bar{z}^2)$

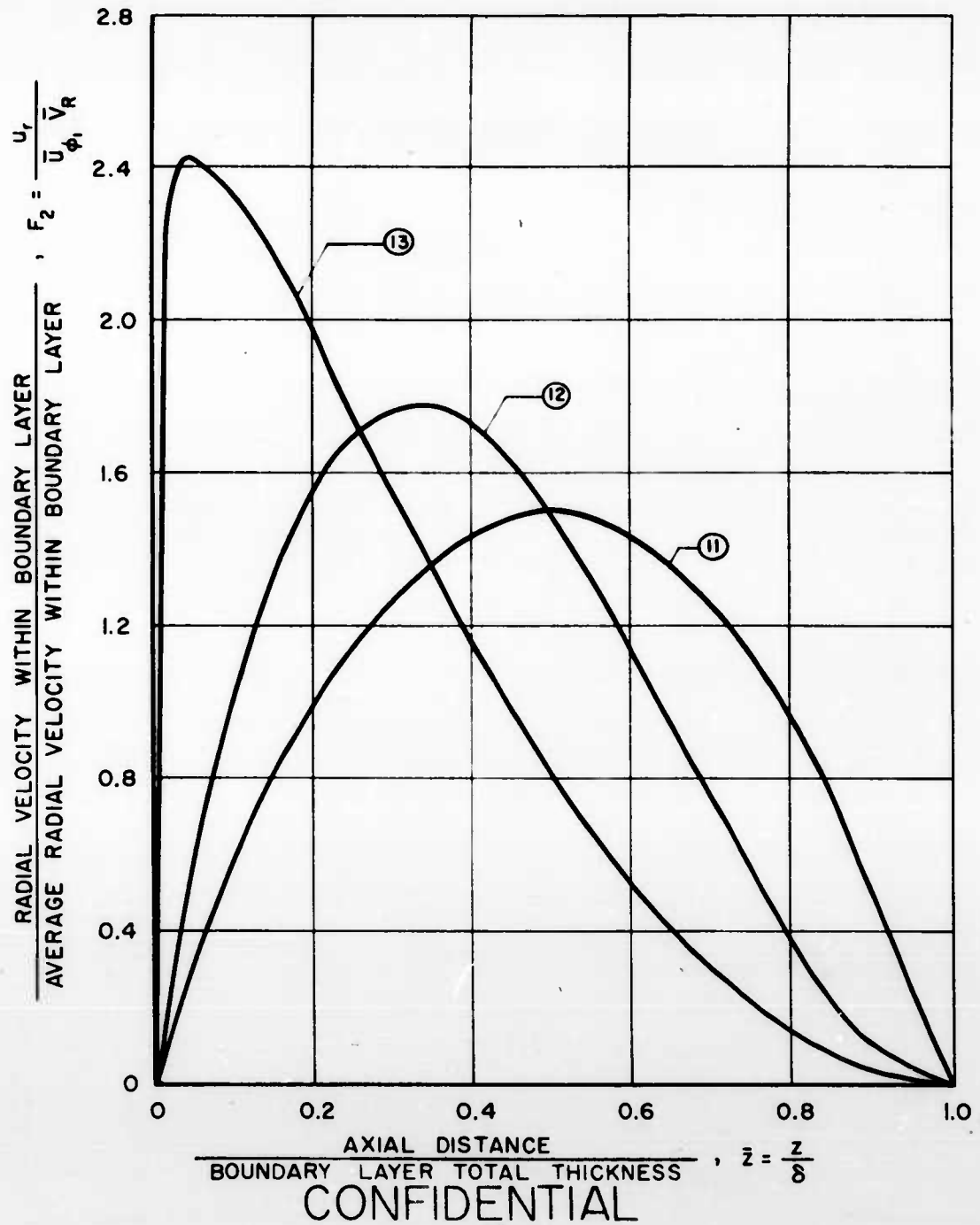

CONFIDENTIAL

VARIATION OF RADIAL MASS FLOW WITH REYNOLDS NUMBER FOR A STRONG VORTEX

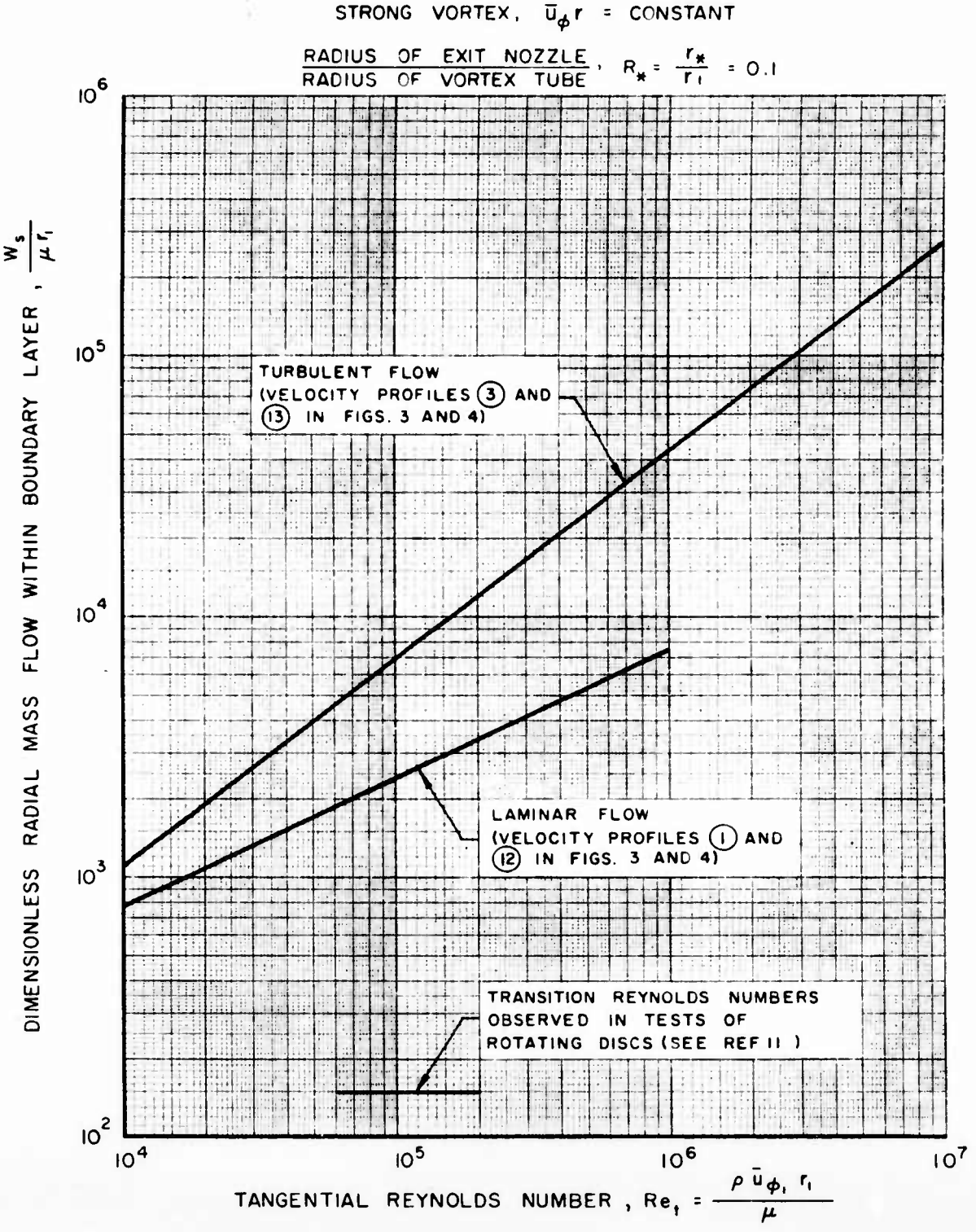

CONFIDENTIAL

FIG. 6

VARIATION WITH RADIUS OF RADIAL MASS FLOW WITHIN BOUNDARY LAYER ON ONE END WALL OF VORTEX TUBE

STRONG VORTEX, $\bar{u}_\phi r$ = CONSTANT

FOR LAMINAR FLOW, $W_{SL} = 2\pi\mu r_1 K_L \sqrt{Re_t}$ EQ (6)

FOR TURBULENT FLOW, $W_{ST} = 2\pi\mu r_1 K_T Re_t^{0.8}$ EQ (8)

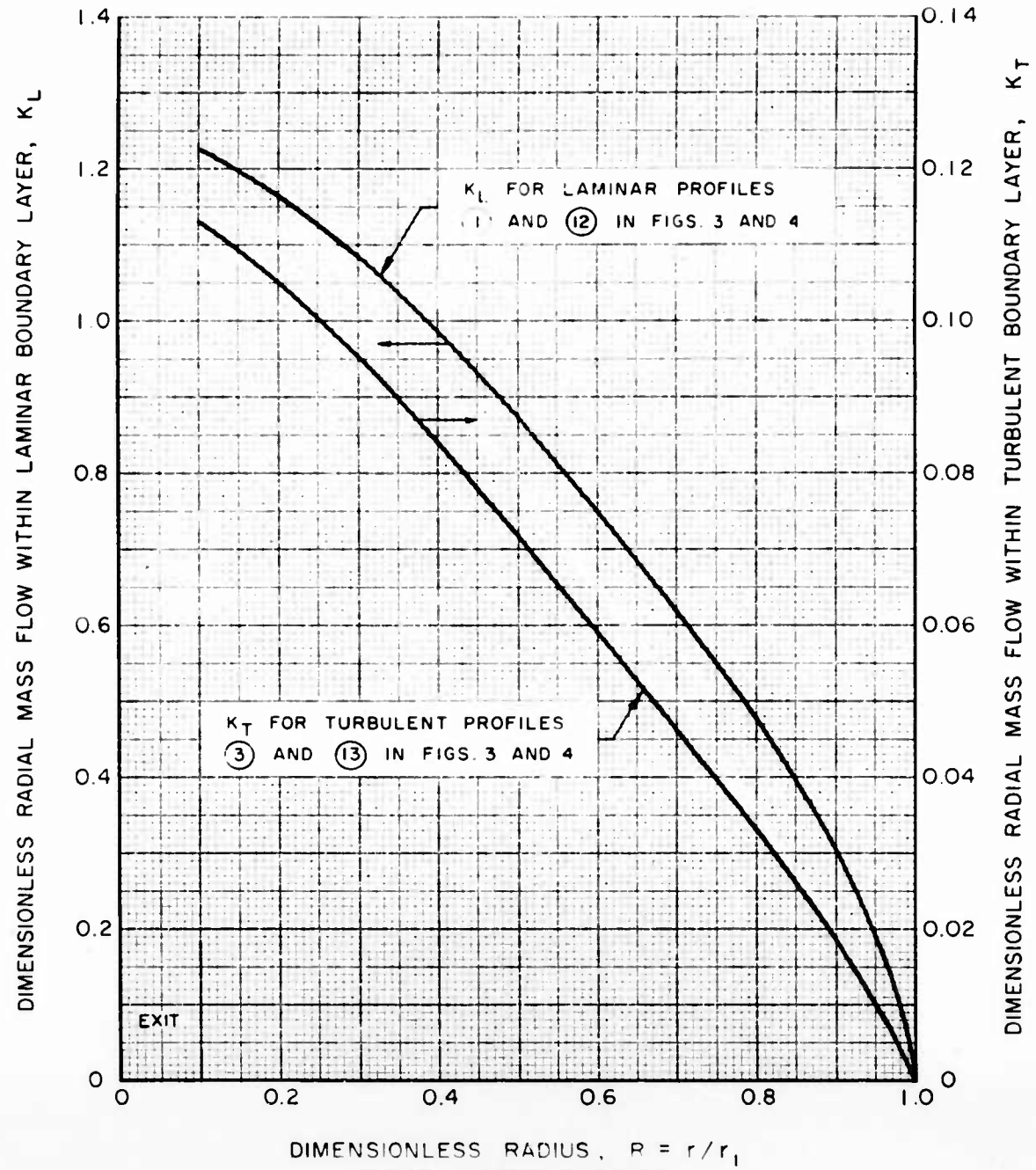

CONFIDENTIAL

VARIATION OF BOUNDARY LAYER THICKNESS WITH RADIUS ON ONE END WALL OF VORTEX TUBE

STRONG VORTEX, $\bar{u}_\phi r$ = CONSTANT

FOR LAMINAR FLOW, $\delta / r_1 = \zeta_L / \sqrt{Re_1}$ EQ (9)

FOR TURBULENT FLOW, $\delta / r_1 = \zeta_T / Re_1^{0.2}$ EQ (10)

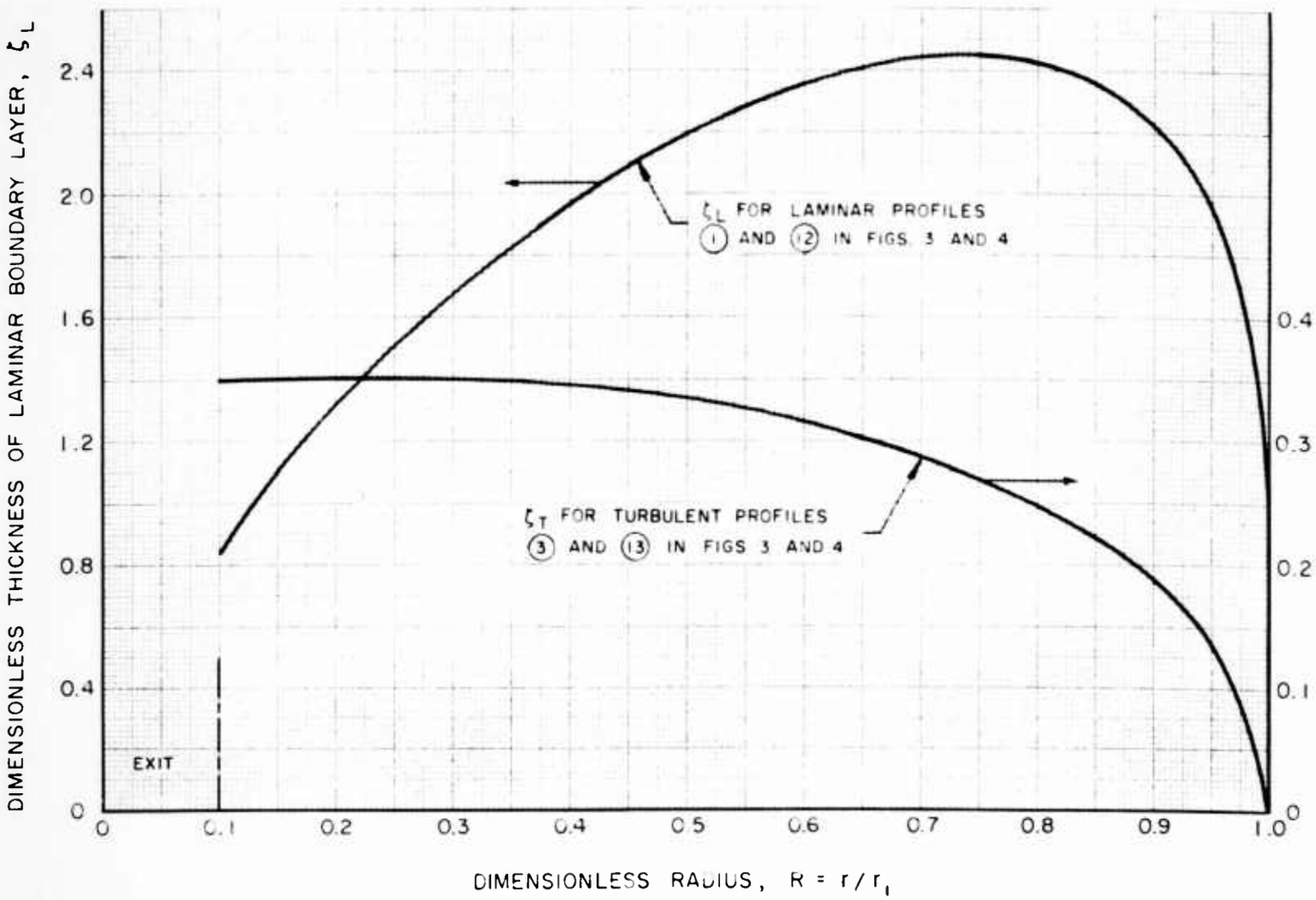

CONFIDENTIAL

CONFIDENTIAL

R-2494-1

FIG. 7

FIG. 8

EFFECT OF RADIAL REYNOLDS NUMBER ON VARIATION OF TANGENTIAL VELOCITY WITH RADIUS FOR THE CASE OF NO SECONDARY FLOW

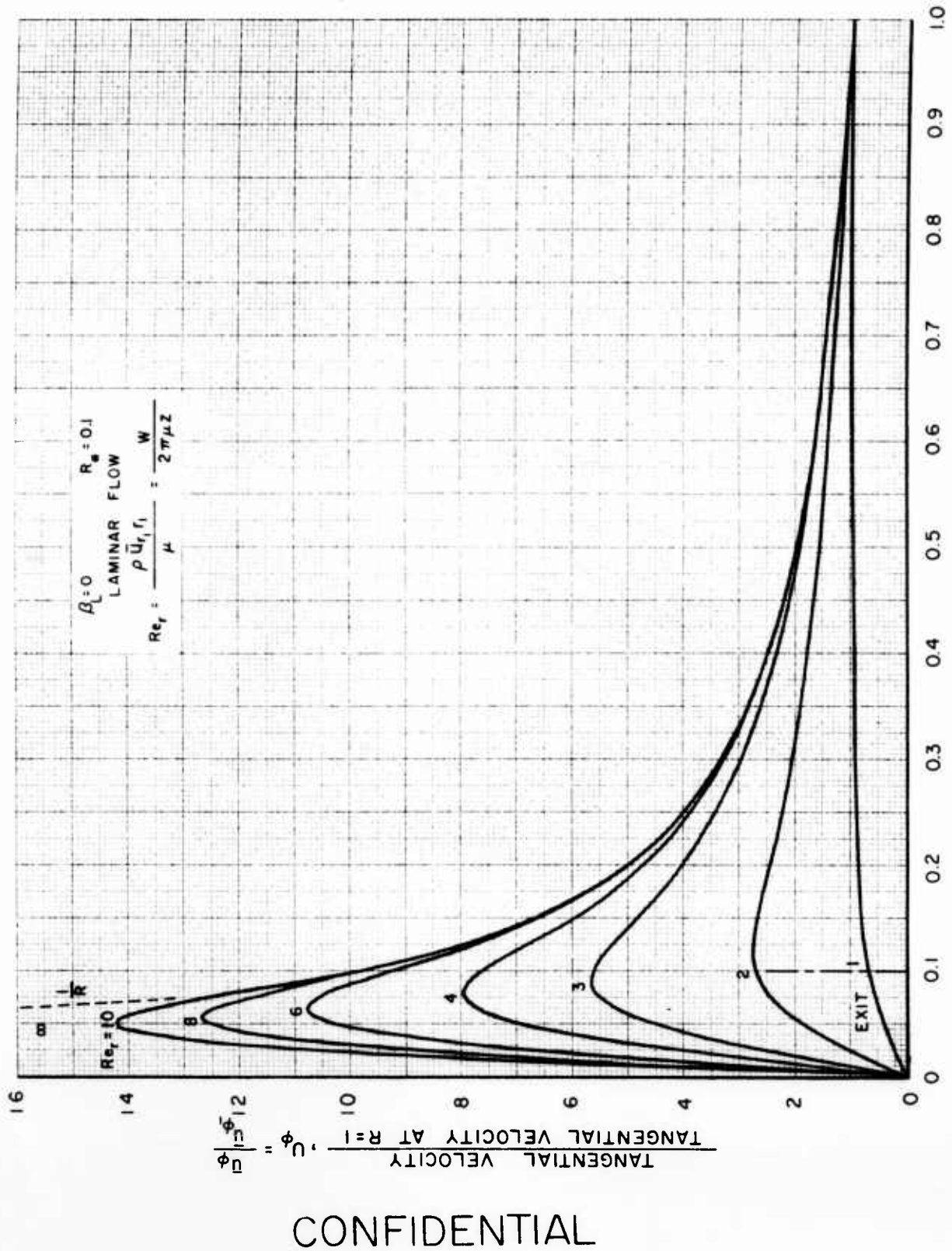

CONFIDENTIAL

MAXIMUM VALUES OF SECONDARY FLOW PARAMETER FOR APPLICABILITY OF STRONG-VORTEX RESULTS

$R_* = 0.1$

$$\beta_L = \frac{2}{\sqrt{Re_r}} \frac{\bar{u}\phi_1}{\bar{u}r_1} \frac{r_1}{z_1} \qquad \beta_T = \frac{2}{Re_r^{1/5}} \frac{\bar{u}\phi_1}{\bar{u}r_1} \frac{r_1}{z_1}$$

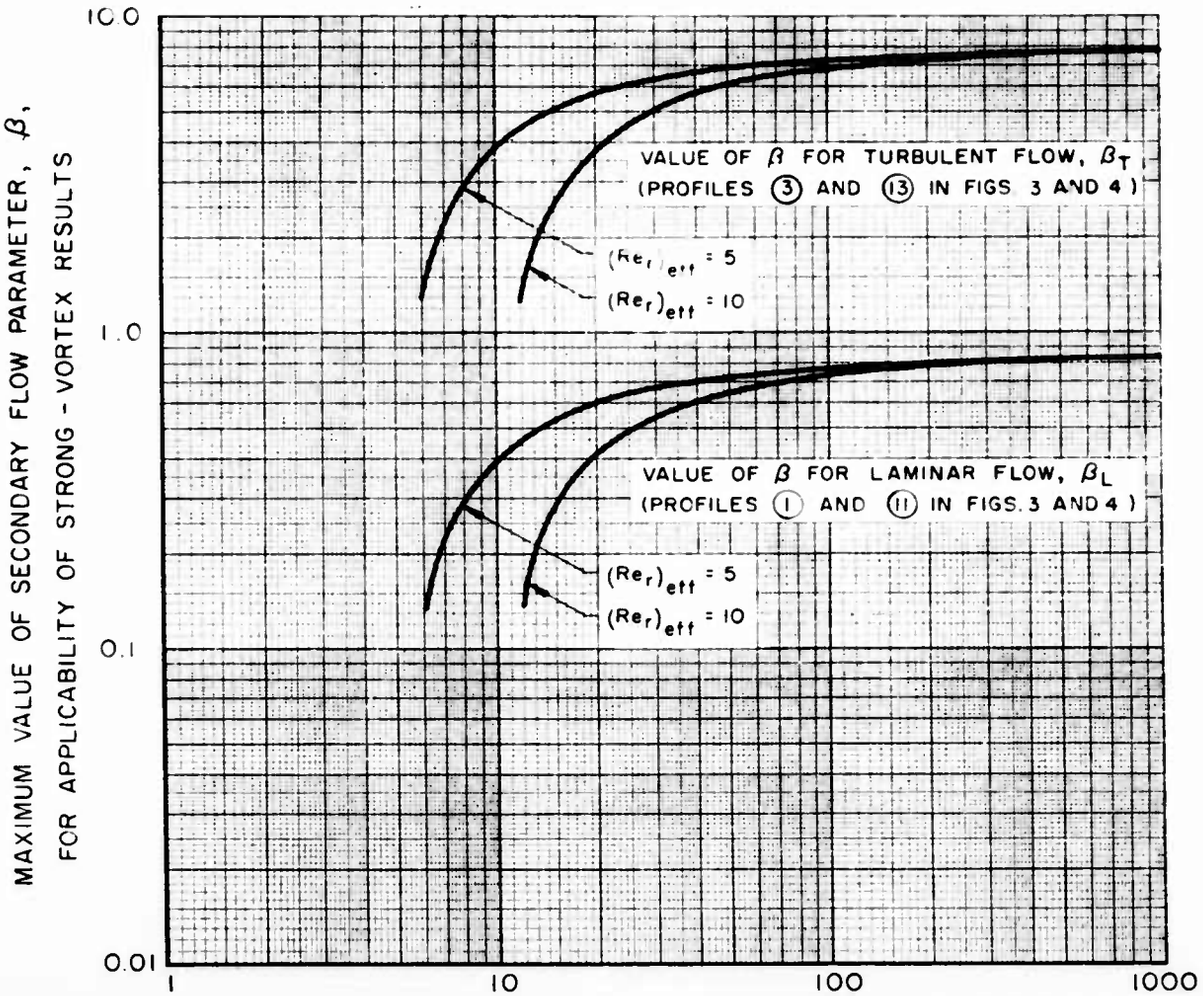

RADIAL REYNOLDS NUMBER, $Re_r = \frac{\rho \bar{u}_{r_1} r_1}{\mu}$

CONFIDENTIAL

CONFIDENTIAL

FIG. 10

APPROXIMATE MAXIMUM VALUES OF TANGENTIAL REYNOLDS NUMBER FOR APPLICABILITY OF STRONG-VORTEX RESULTS

$R_* = 0.1$ $\qquad (Re_r)_{eff} = 5$

CURVES CALCULATED FROM PROFILES (1), (3), (12) AND (13) IN FIGS. 3 AND 4

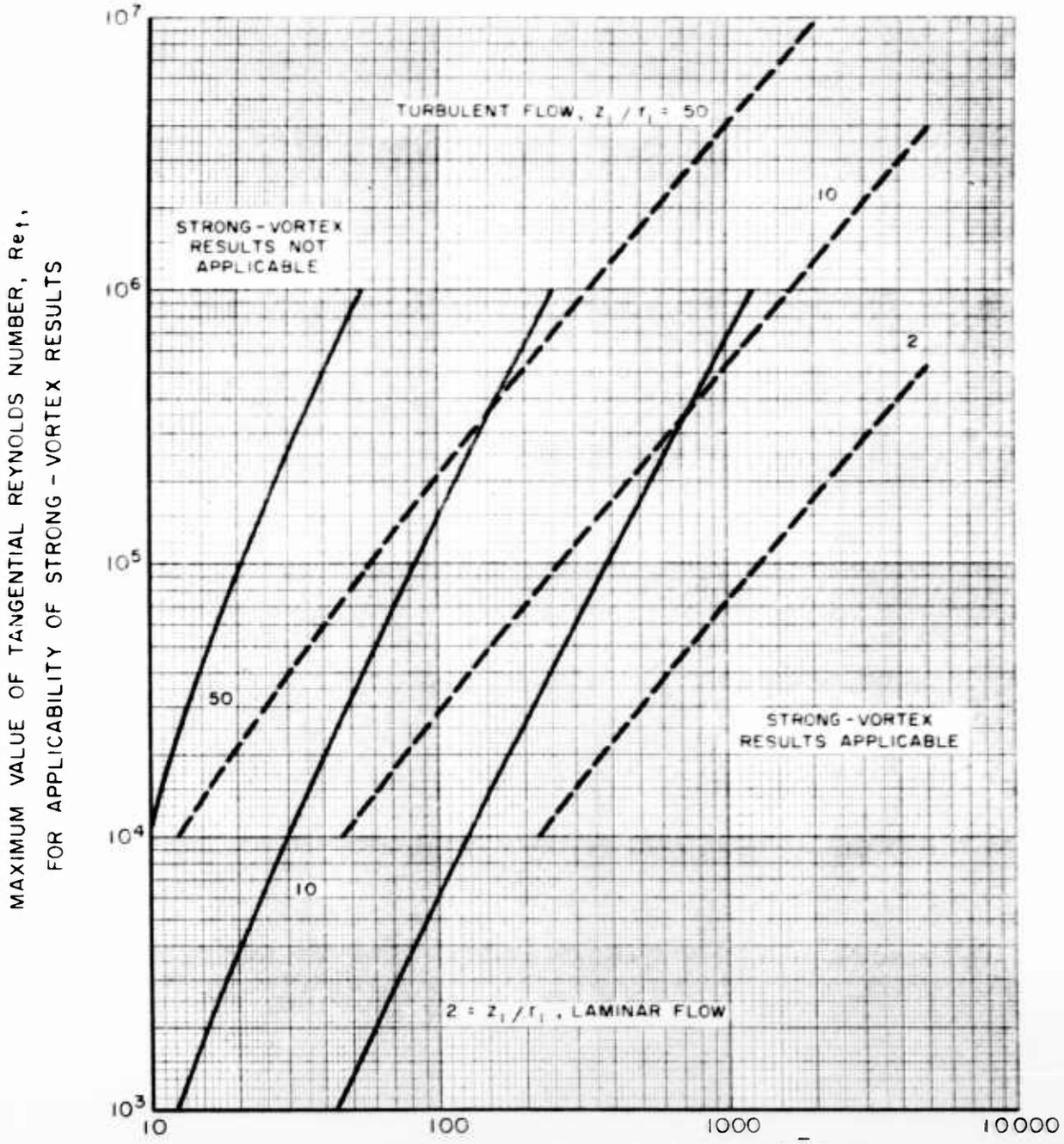

CONFIDENTIAL

CONFIDENTIAL

COMPARISON OF SECONDARY FLOW AND TOTAL FLOW IN VORTEX TUBE

IMPLICATIONS OF DATA DISCUSSED IN TEXT

SYMBOL	TUBE DIAMETER, d—IN	SOURCE
○	0.6	REFS 3,4
□	1.0	
△	2.0	
×	6.0	REF 5

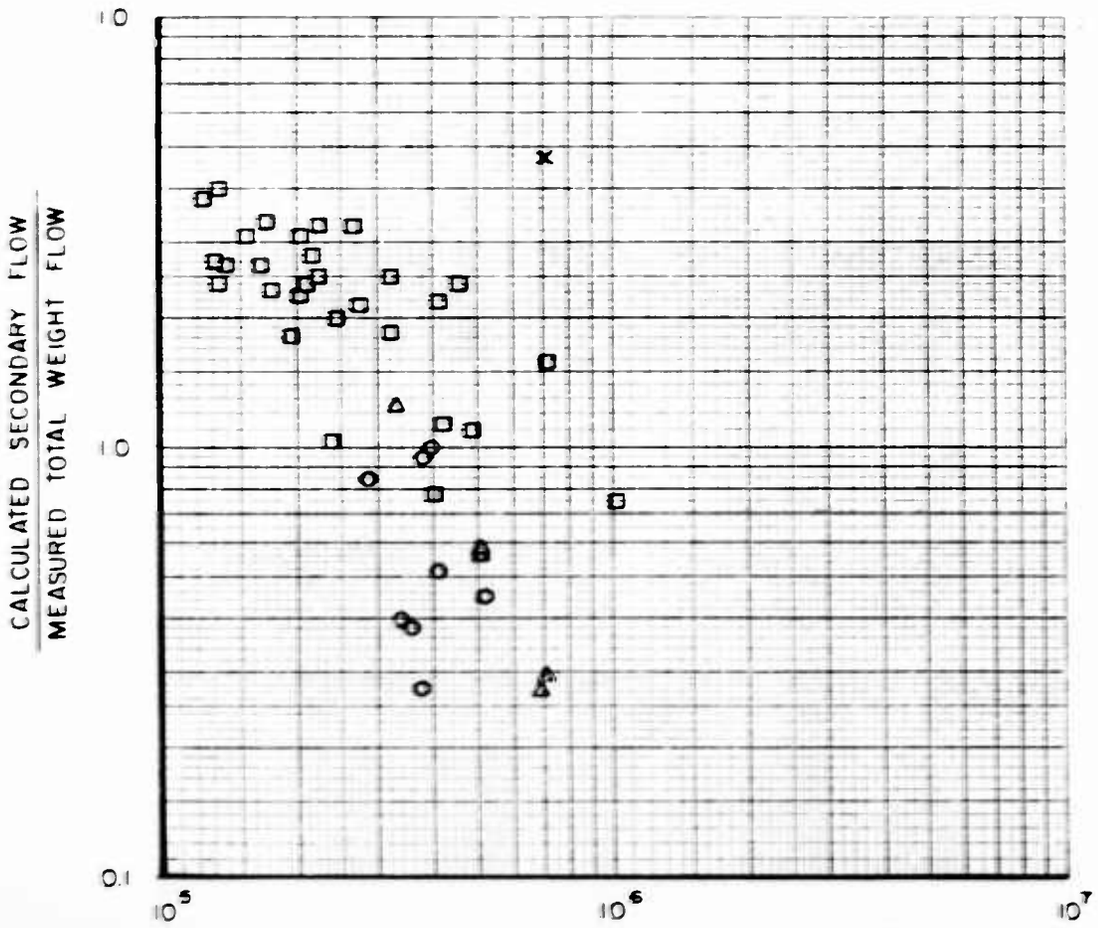

CONFIDENTIAL

CONFIDENTIAL

EFFECT OF RADIUS ON ANGULAR MOMENTUM IN PRIMARY FLOW FOR A RADIAL REYNOLDS NUMBER OF 10

LAMINAR FLOW PROFILES (1) AND (12) IN FIGS 3 AND 4

$$R_e = 0.1$$

$$\beta_L = \frac{2}{\sqrt{Re_1}} \frac{\bar{u}_{\phi_1}}{\bar{u}_{r_1}} \frac{r_1}{z_1}$$

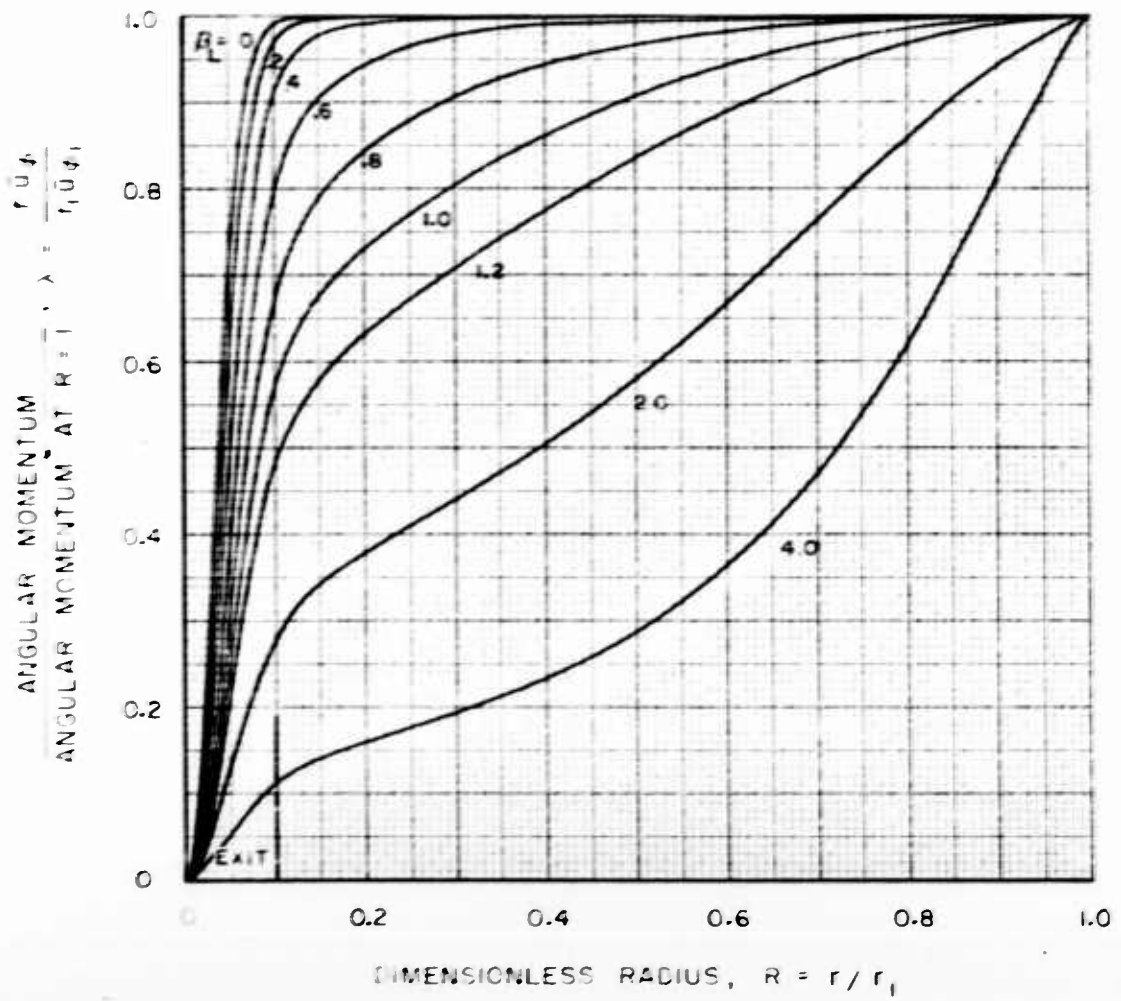

CONFIDENTIAL

CONFIDENTIAL

FIG. 13

EFFECT OF RADIUS ON TANGENTIAL VELOCITY IN PRIMARY FLOW FOR A RADIAL REYNOLDS NUMBER OF 10

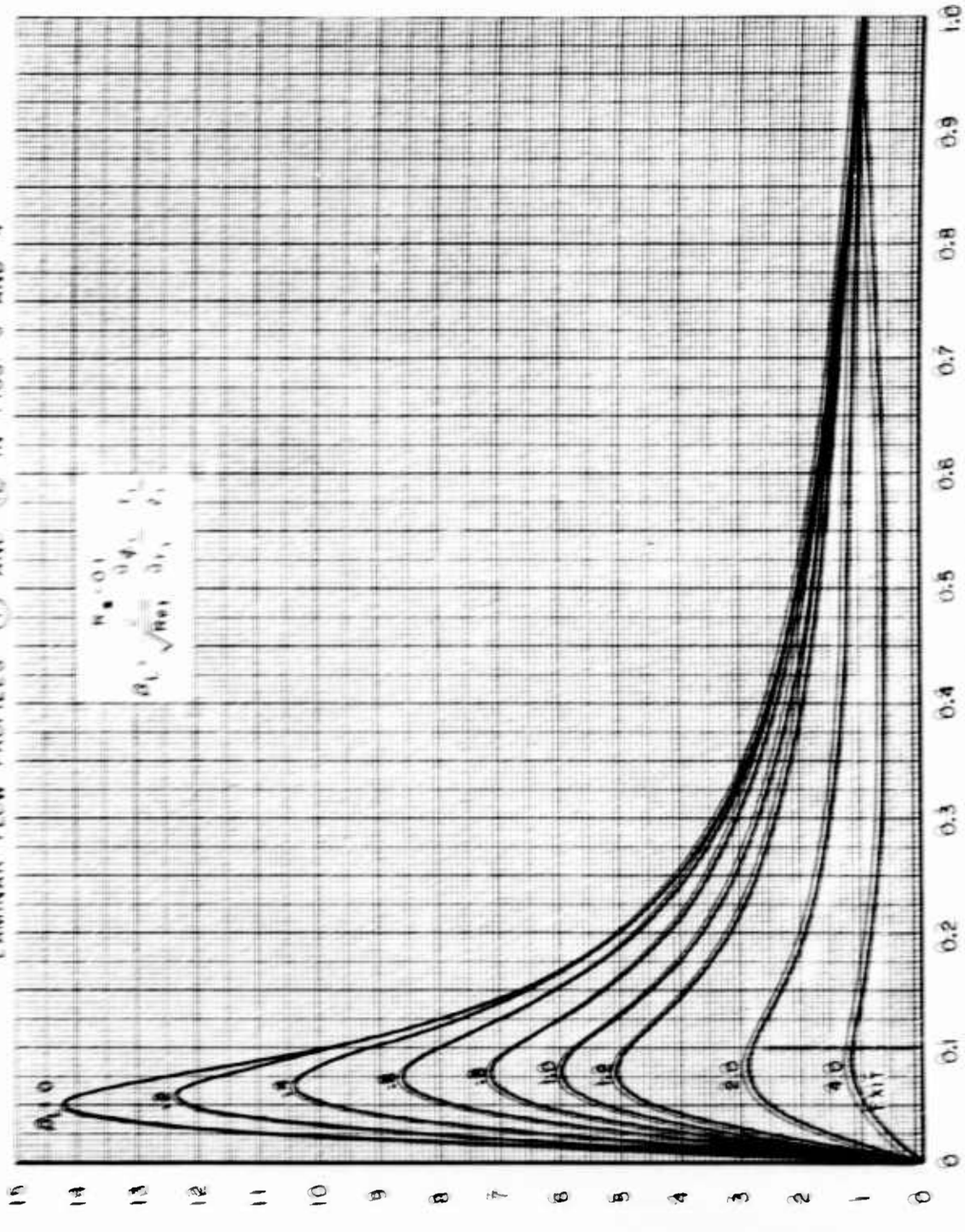

CONFIDENTIAL

CONFIDENTIAL

FIG. 14

EFFECT OF RADIUS ON STATIC PRESSURE COEFFICIENT FOR A RADIAL REYNOLDS NUMBER OF 10

LAMINAR FLOW PROFILES (1) AND (12) IN FIGS. 3 AND 4

$R_e = 0.1$

$$\beta_L = \frac{2}{\sqrt{Re_1}} \frac{\partial \phi_1}{\partial r_1} \frac{r_1}{z_1}$$

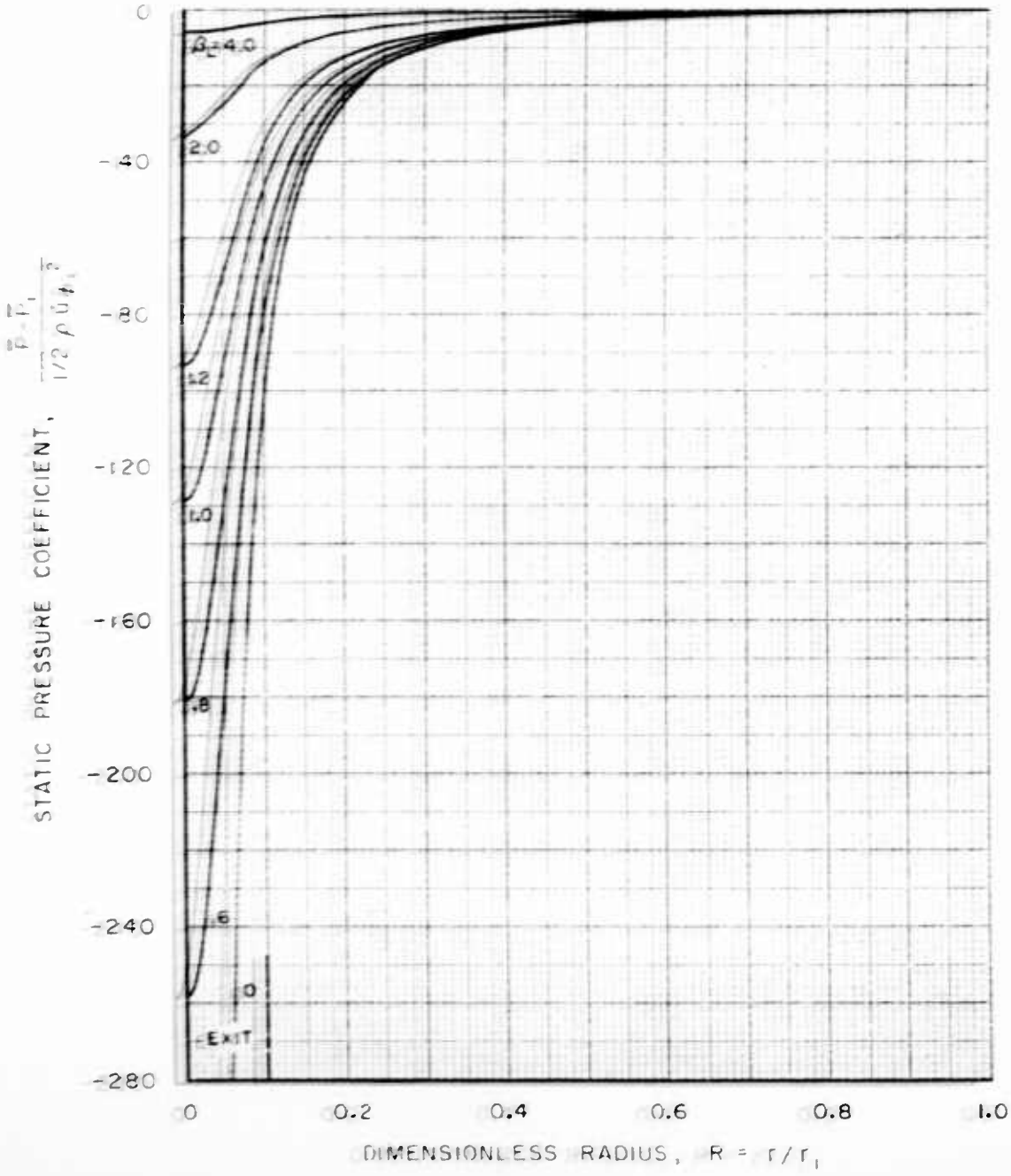

CONFIDENTIAL

CONFIDENTIAL

FIG. 15

EFFECT OF RADIUS ON SECONDARY FLOW WITHIN THE BOUNDARY LAYER FOR A RADIAL REYNOLDS NUMBER OF 10

LAMINAR FLOW PROFILES (1) AND (12) IN FIGS. 3 AND 4

$R_* = 0.1$

$$\beta_L = \frac{2}{\sqrt{Re_t}} \frac{\bar{u}_{\phi_1}}{\bar{u}_{r_1}} \frac{r_1}{z_1}$$

$$w_{SL} = 2\pi r_1 \mu K_L \sqrt{Re_t} \qquad \text{EQ (6)}$$

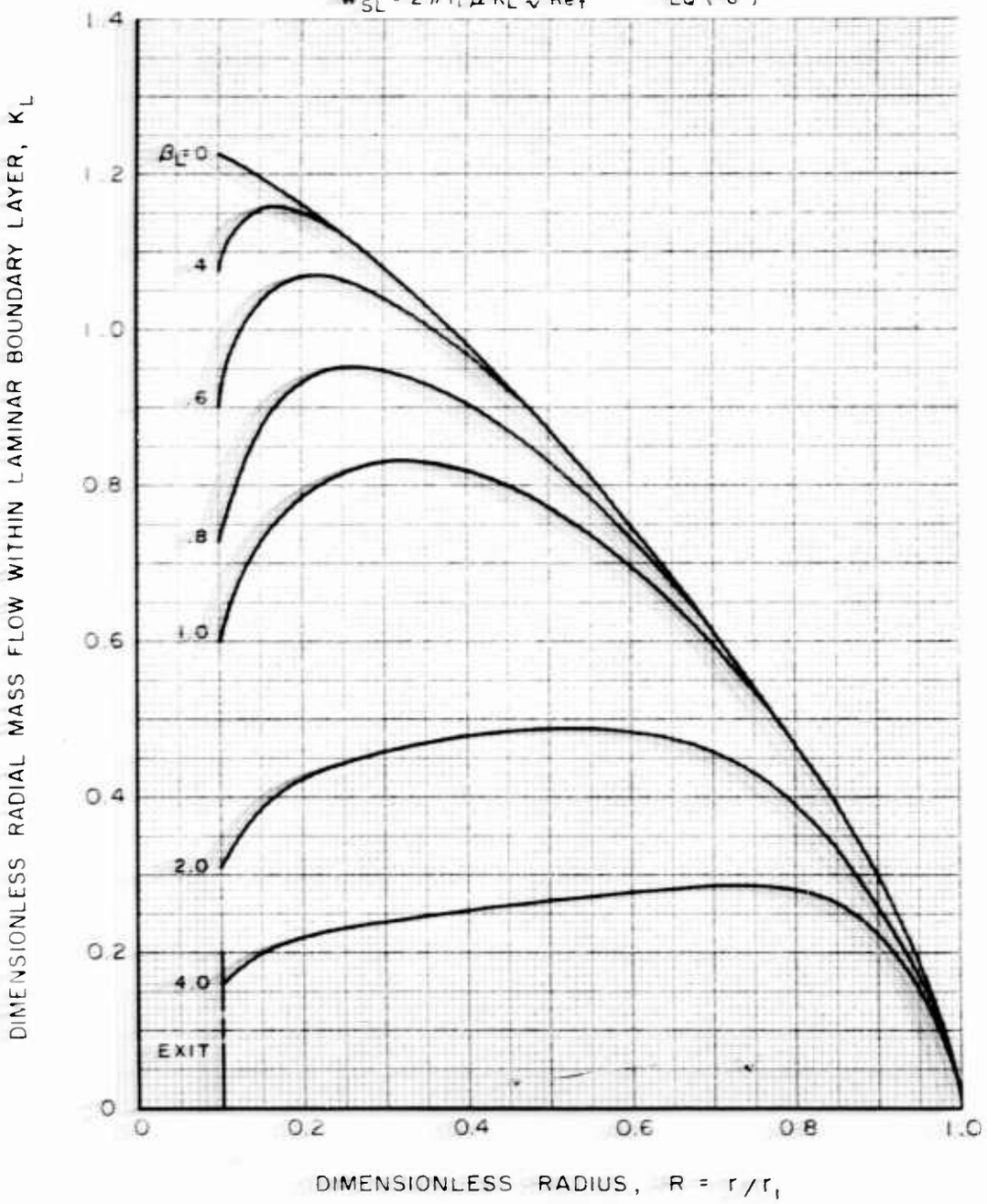

CONFIDENTIAL

CONFIDENTIAL

FIG. 16

EFFECT OF RADIUS ON FRACTION OF TOTAL FLOW WITHIN BOUNDARY LAYERS ON BOTH END WALLS FOR A RADIAL REYNOLDS NUMBER OF 10

LAMINAR FLOW PROFILES (1) AND (12) IN FIGS. 3 AND 4

$R_* = 0.1$

$$\beta_L = \frac{2}{\sqrt{Re_1}} \frac{\bar{u}_{\phi_1}}{\bar{u}_{r_1}} \frac{r_1}{z_1}$$

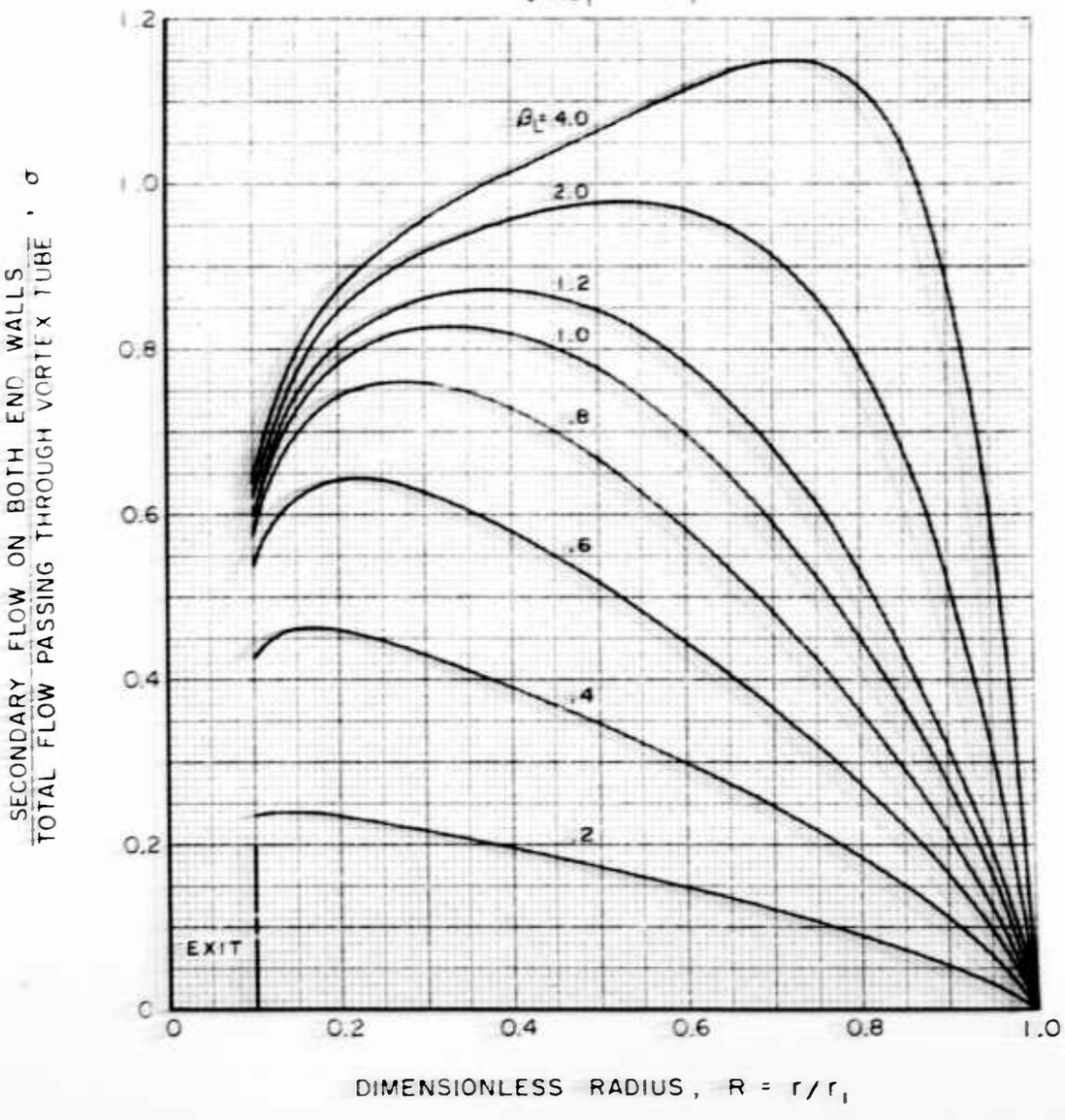

CONFIDENTIAL

CONFIDENTIAL

FIG. 17

EFFECT OF RADIUS ON BOUNDARY LAYER THICKNESS ON END WALL FOR A RADIAL REYNOLDS NUMBER OF 10

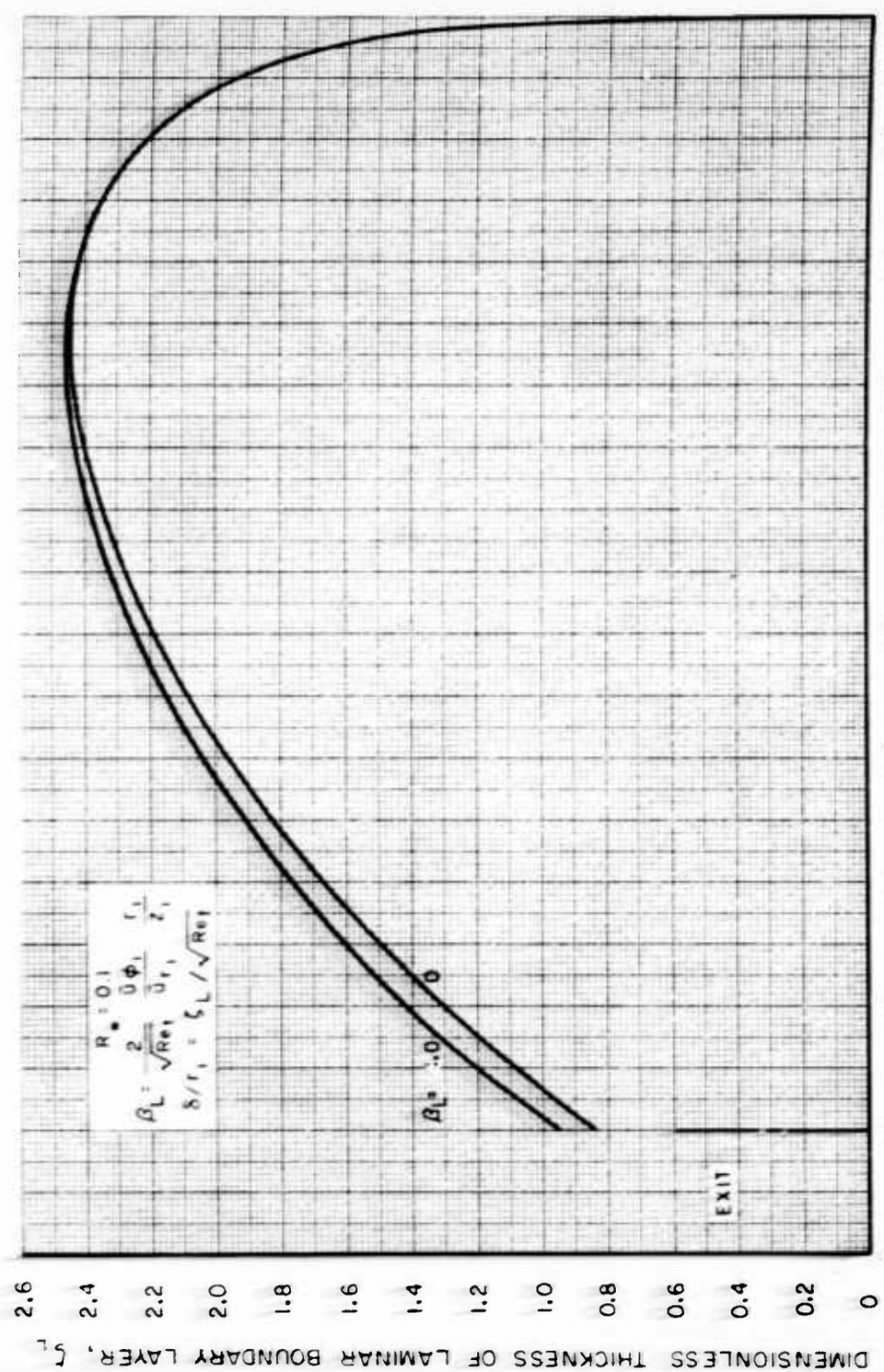

CONFIDENTIAL

FLOW STREAMLINES FOR RADIAL REYNOLDS NUMBER OF 10 WITH MODERATE SECONDARY FLOW

LAMINAR FLOW, PROFILES (1) AND (12) IN FIGURES 3 AND 4

$$\beta_L = \frac{2}{\sqrt{Re_1}} \frac{\bar{u}_{\phi_1}}{\bar{u}_{r_1}} \frac{r_1}{Z_1} = 0.4$$

$R_* = 0.1$ $\quad \frac{Z_1}{r_1} = 6.0$ $\quad Re_1 = 144$ $\quad \frac{\bar{u}_{\phi_1}}{\bar{u}_{r_1}} = 14.4$

$\sigma_M = 0.46$ $\quad \sigma_* = 0.43$ $\quad \sigma_R = 0.03$

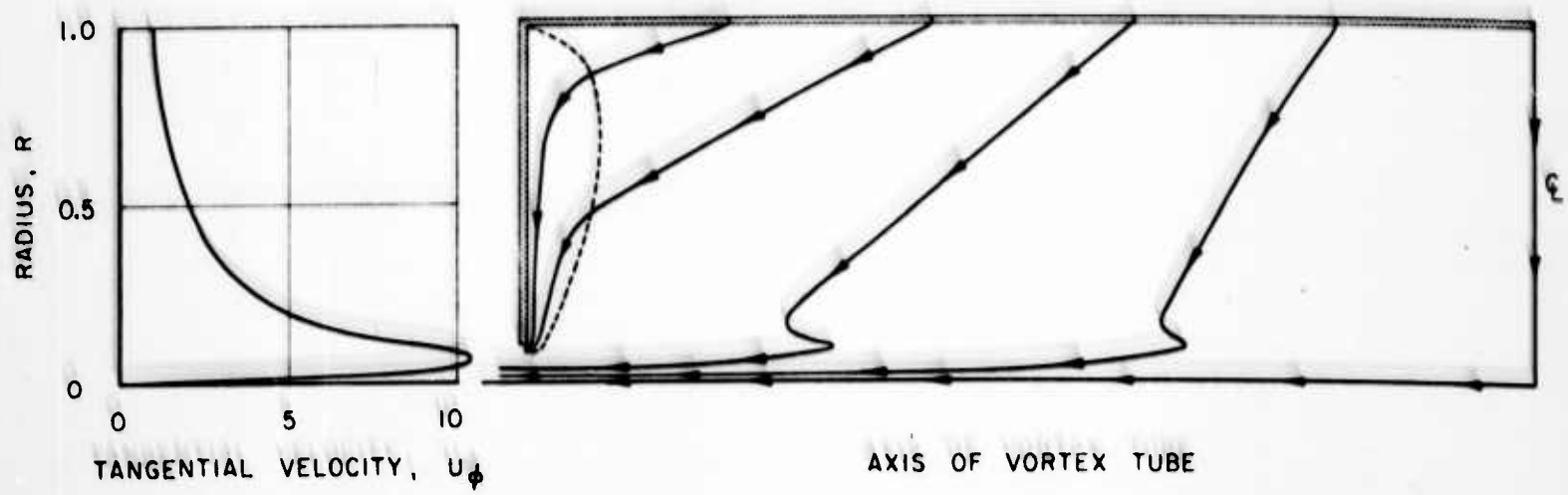

FLOW STREAMLINES FOR RADIAL REYNOLDS NUMBER OF 10 WITH LARGE SECONDARY FLOW

LAMINAR FLOW, PROFILES (1) AND (12) IN FIGURES 3 AND 4

$$\beta_L = \frac{2}{\sqrt{Re_1}} \frac{\bar{u}_{\phi_1}}{\bar{u}_{r_1}} \frac{r_1}{Z_1} = 1.0$$

$R_* = 0.1$ $\quad \frac{Z_1}{r_1} = 6.0$ $\quad Re_1 = 900$ $\quad \frac{\bar{u}_{\phi_1}}{\bar{u}_{r_1}} = 90$

$\sigma_M = 0.82$ $\quad \sigma_* = 0.59$ $\quad \sigma_R = 0.23$

FLOW STREAMLINES FOR RADIAL REYNOLDS NUMBER OF 10 WITH A VORTEX CELL

LAMINAR FLOW, PROFILES (1) AND (12) IN FIGURES 3 AND 4

$$\beta_L = \frac{2}{\sqrt{Re_t}} \frac{\bar{u}_{\phi_1}}{\bar{u}_{r_1}} \frac{r_1}{Z_1} = 4.0$$

$R_* = 0.1$ $\quad \frac{Z_1}{r_1} = 6.0$ $\quad Re_t = 14{,}400$ $\quad \frac{\bar{u}_{\phi_1}}{\bar{u}_{r_1}} = 1440$

$\sigma_M = 1.0$ $\quad \sigma_* = 0.63$ $\quad \sigma_R = 0.37$

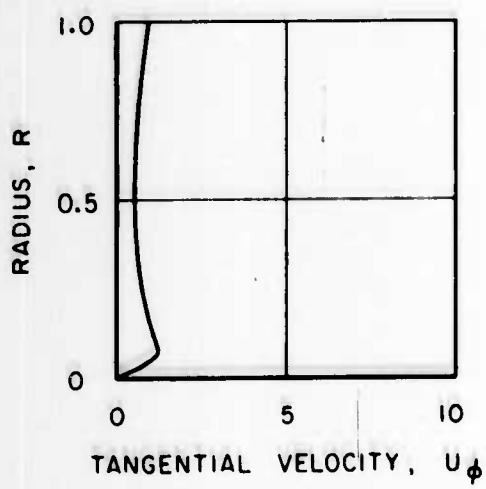

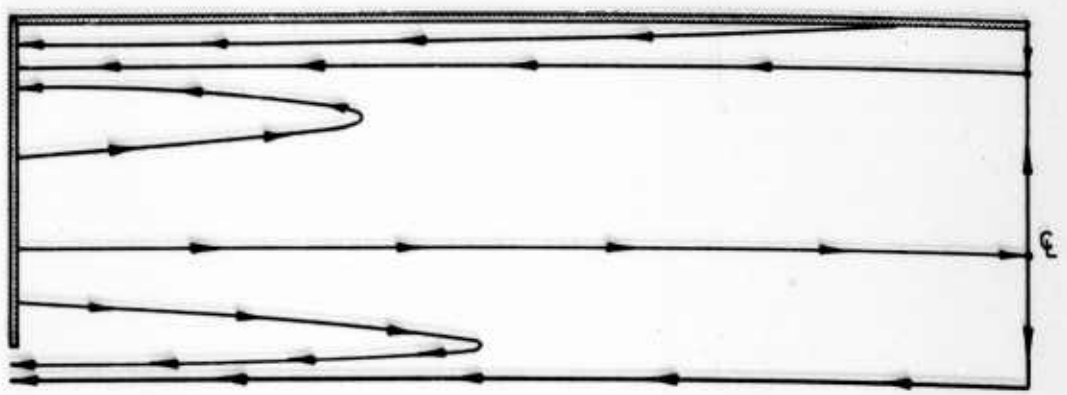

AXIS OF VORTEX TUBE

R-2494-1

FIG. 20

EFFECT OF RADIUS ON ANGULAR MOMENTUM IN PRIMARY FLOW FOR A RADIAL REYNOLDS NUMBER OF 5

LAMINAR FLOW PROFILES (1) AND (12) IN FIGS. 3 AND 4

$R_* = 0.1$

$$\beta_L = \frac{2}{\sqrt{Re_t}} \frac{\bar{u}_{\phi_1}}{\bar{u}_{r_1}} \frac{r_1}{z_1}$$

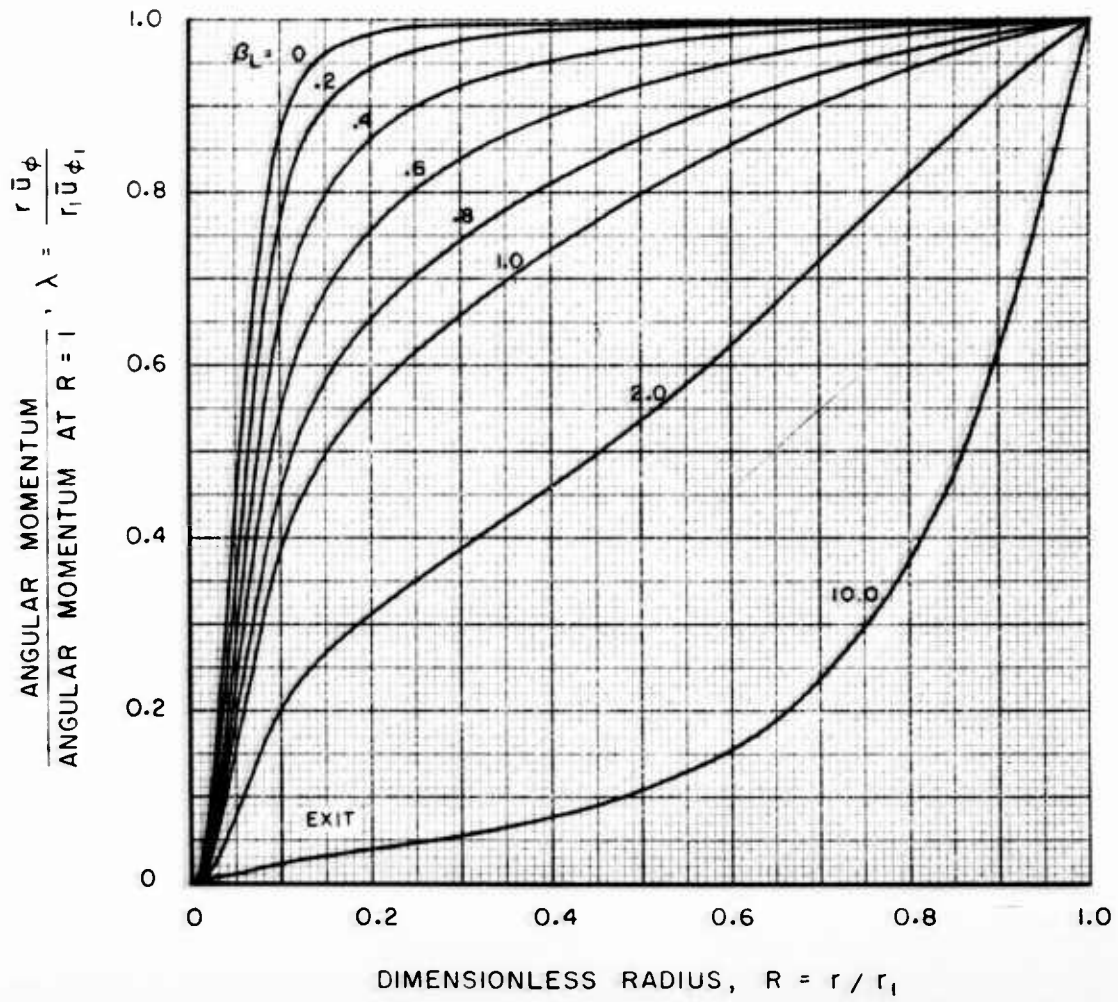

EFFECT OF RADIUS ON TANGENTIAL VELOCITY IN PRIMARY FLOW FOR A RADIAL REYNOLDS NUMBER OF 5

LAMINAR FLOW PROFILES (1) AND (12) IN FIGS. 3 AND 4

$R_* = 0.1$

$$\beta_L = \frac{2}{\sqrt{Re_t}} \frac{\bar{u}_{\phi_1}}{\bar{u}_{r_1}} \frac{r_1}{z_1}$$

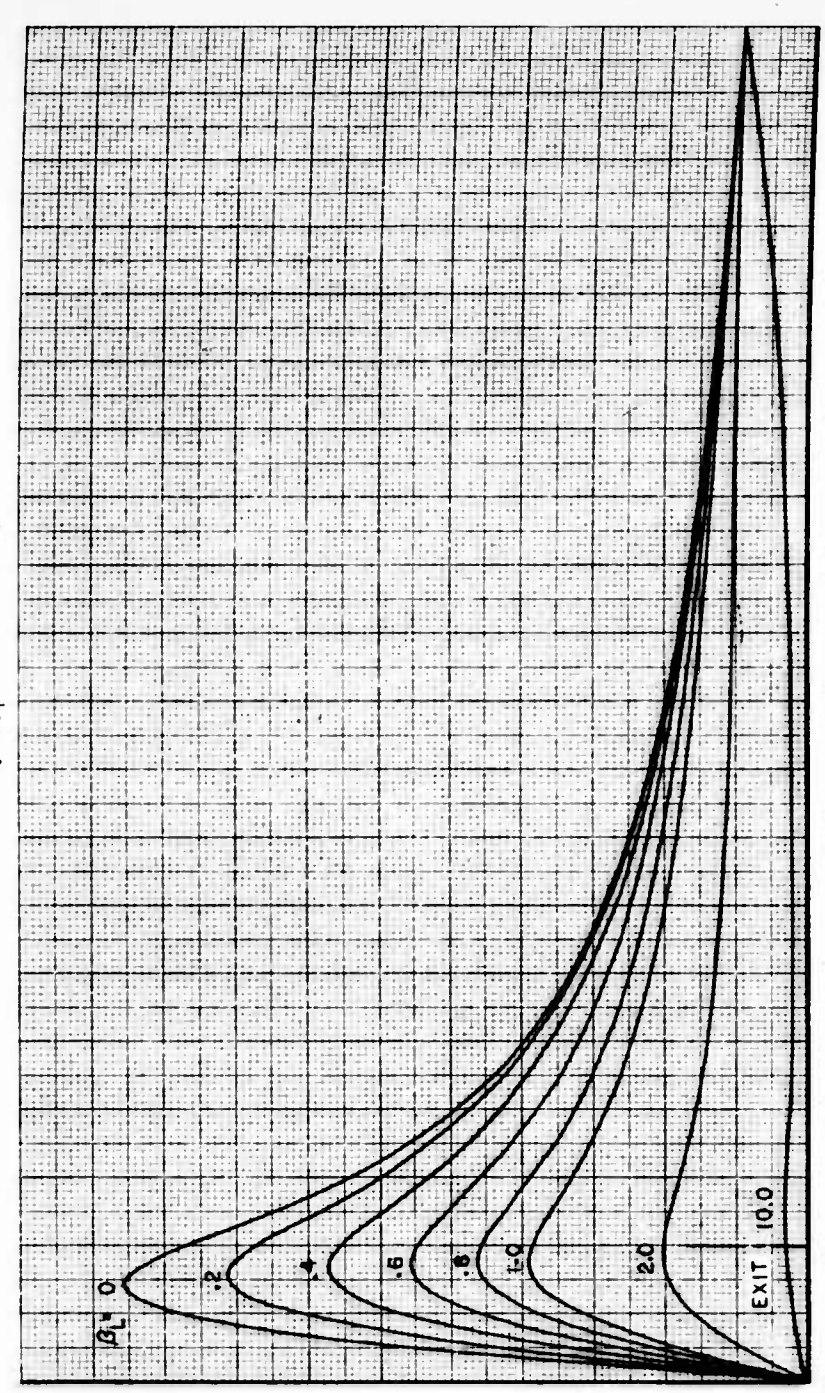

EFFECT OF RADIUS ON FRACTION OF TOTAL FLOW WITHIN BOUNDARY LAYERS ON BOTH END WALLS FOR A RADIAL REYNOLDS NUMBER OF 5

LAMINAR FLOW PROFILES (1) AND (12) IN FIGS. 3 AND 4

$$R_* = 0.1$$

$$\beta_L = \frac{2}{\sqrt{Re_t}} \frac{\bar{u}\phi_1}{\bar{u}r_1} \frac{r_1}{z_1}$$

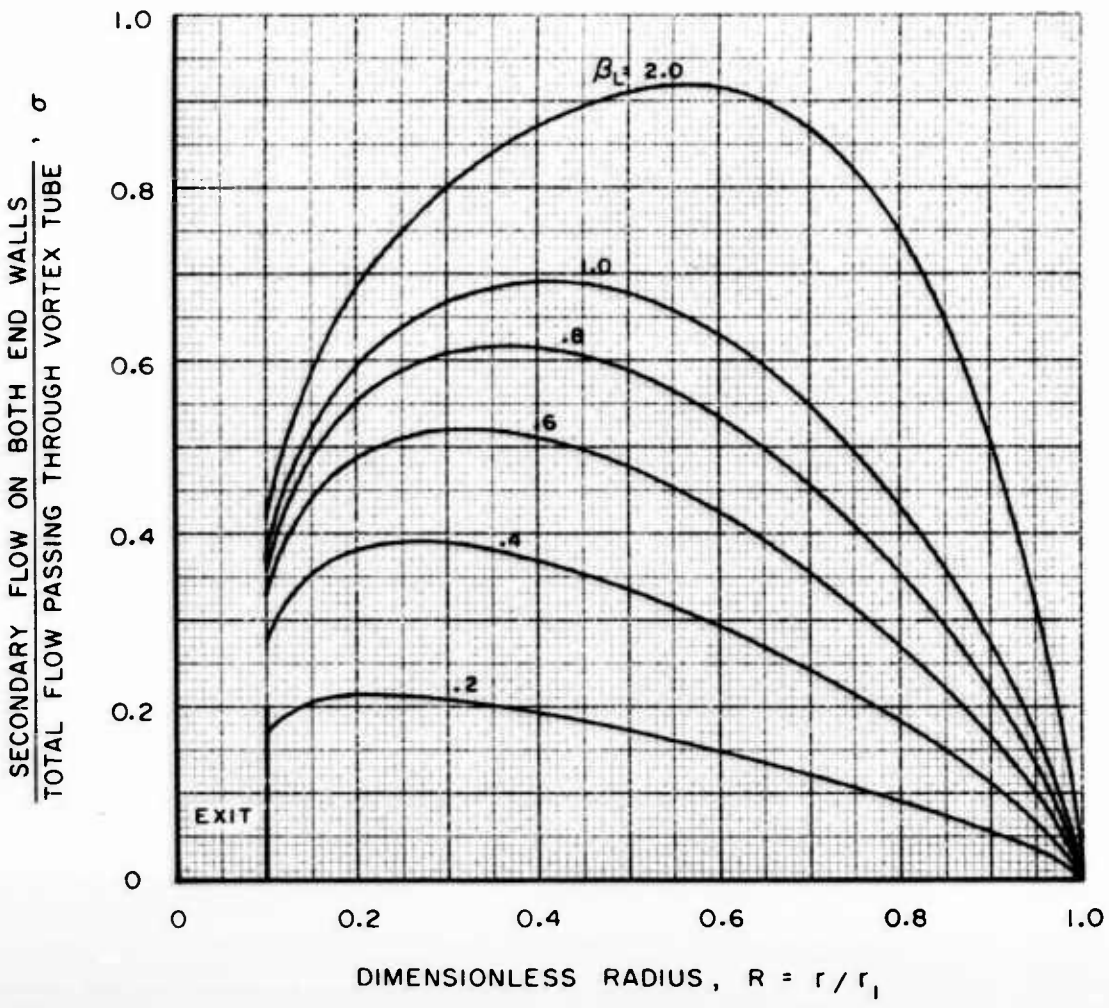

EFFECT OF RADIUS ON BOUNDARY LAYER THICKNESS ON END WALL FOR A RADIAL REYNOLDS NUMBER OF 5

LAMINAR FLOW PROFILES (1) AND (12) IN FIGS. 3 AND 4

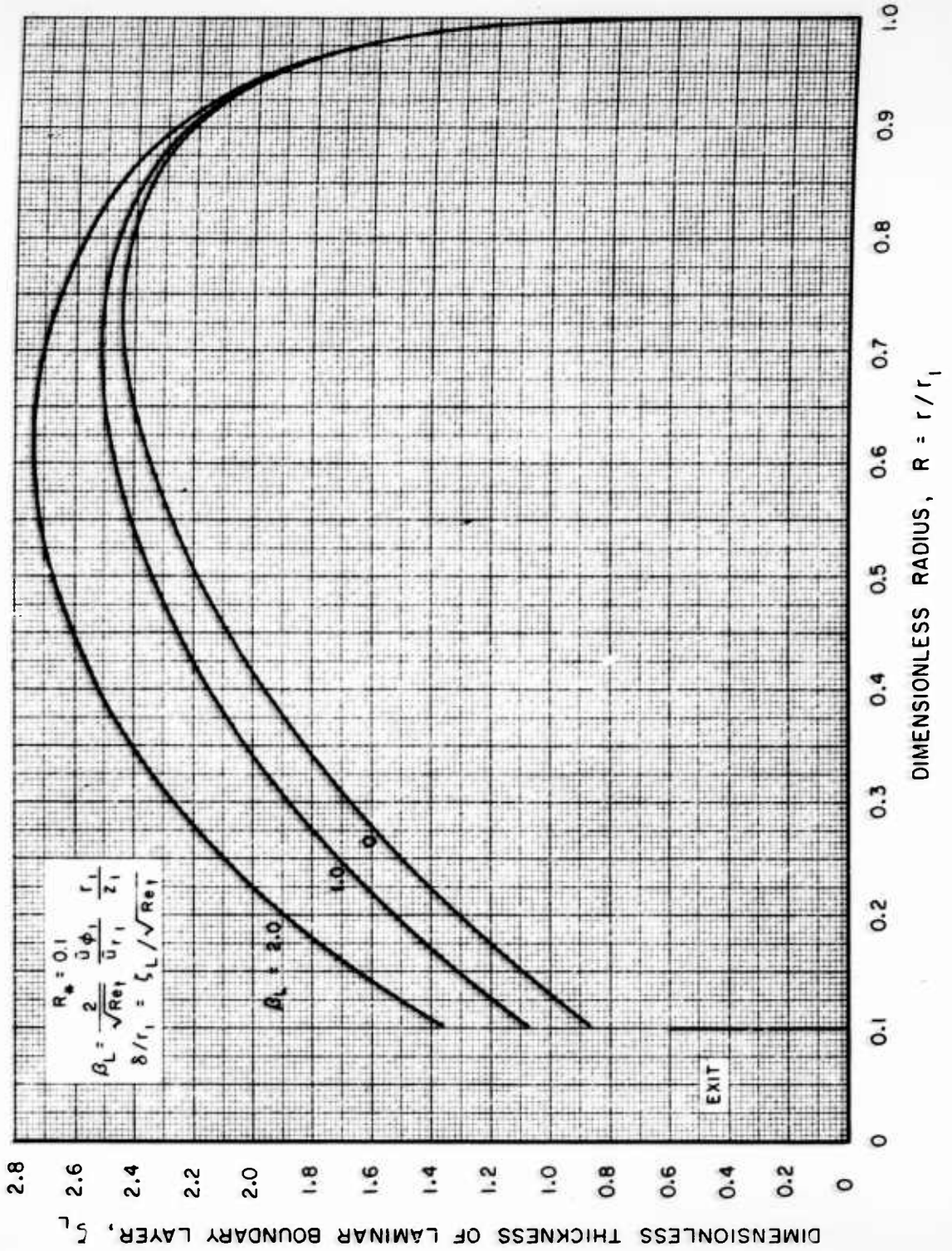

EFFECT OF RADIUS ON ANGULAR MOMENTUM IN PRIMARY FLOW FOR A RADIAL REYNOLDS NUMBER OF 20

LAMINAR FLOW PROFILES (1) AND (2) IN FIGS. 3 AND 4

$R_* = 0.1$

$$\beta_L = \frac{2}{\sqrt{Re_1}} \frac{\bar{u}_{\phi_1}}{\bar{u}_{r_1}} \frac{r_1}{z_1}$$

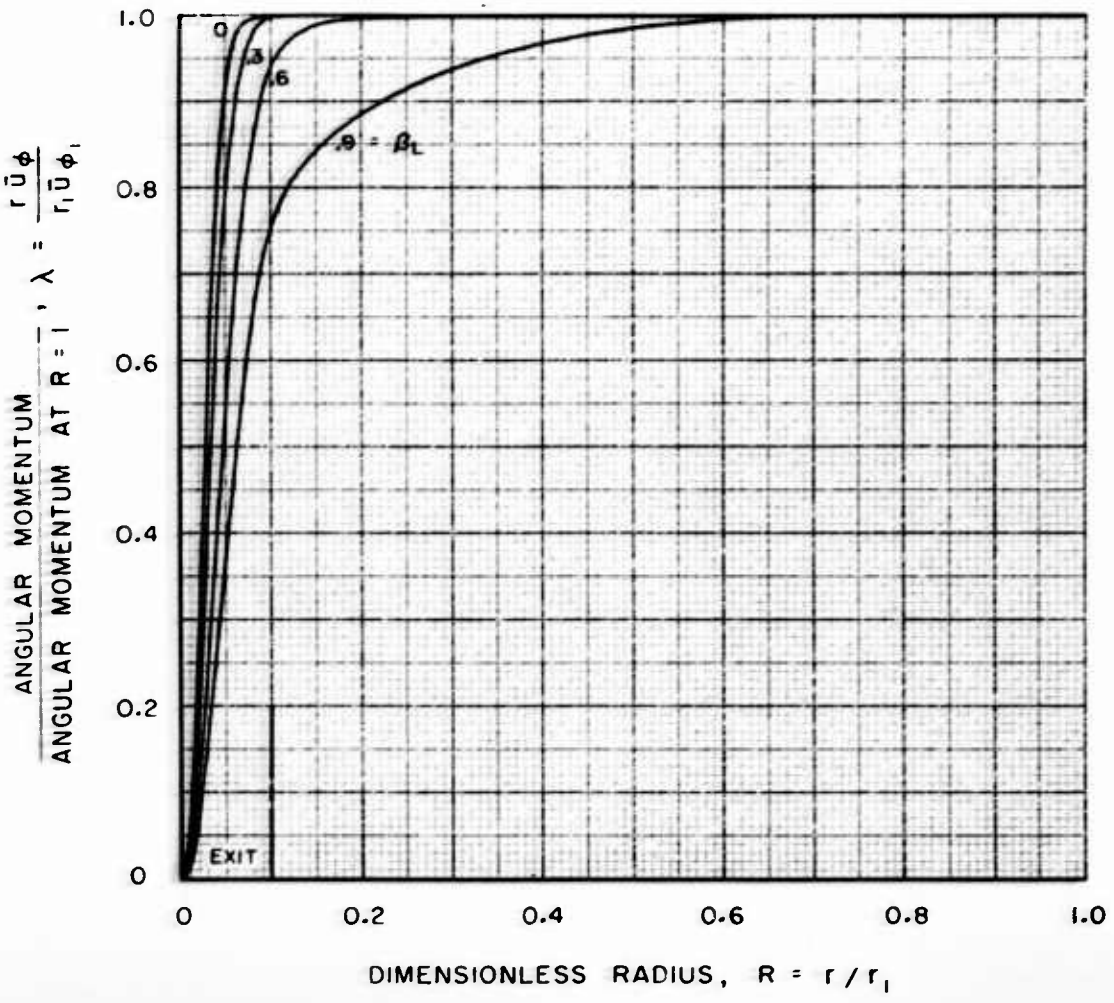

FIG. 26

EFFECT OF RADIUS ON TANGENTIAL VELOCITY IN PRIMARY FLOW FOR A RADIAL REYNOLDS NUMBER OF 20

LAMINAR FLOW PROFILES (1) AND (12) IN FIGS. 3 AND 4

$R_* = 0.1$

$$\beta_L = \frac{2}{\sqrt{Re_1}} \frac{\bar{v}_{\phi_1}}{\bar{u}_{r_1}} \frac{r_1}{z_1}$$

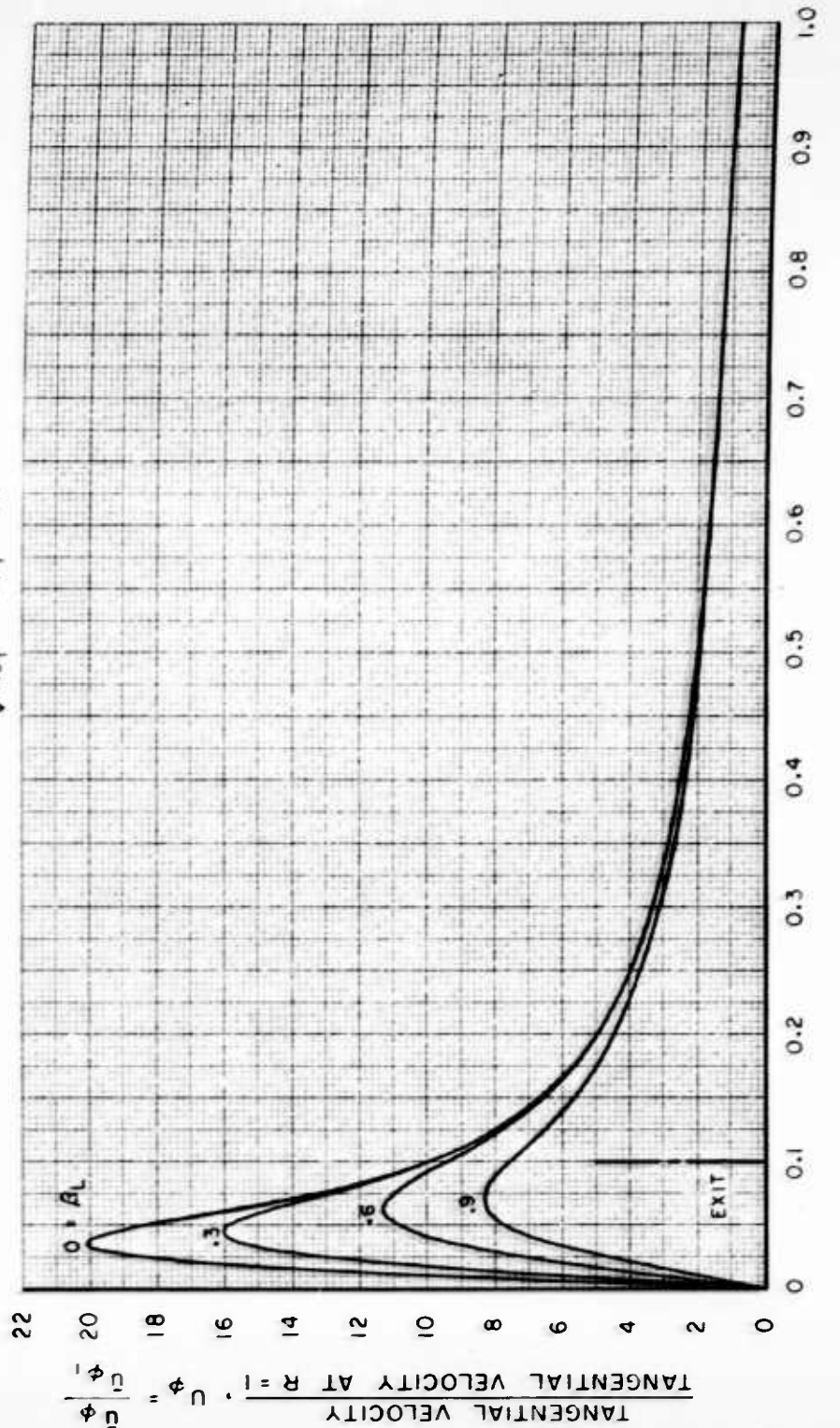

EFFECT OF RADIUS ON FRACTION OF TOTAL FLOW WITHIN BOUNDARY LAYERS ON BOTH END WALLS FOR A RADIAL REYNOLDS NUMBER OF 20

LAMINAR FLOW PROFILES (1) AND (12) IN FIGS. 3 AND 4

$R_* = 0.1$

$$\beta_L = \frac{2}{\sqrt{Re_1}} \frac{\bar{u}_{\phi_1}}{\bar{u}_{r_1}} \frac{r_1}{z_1}$$

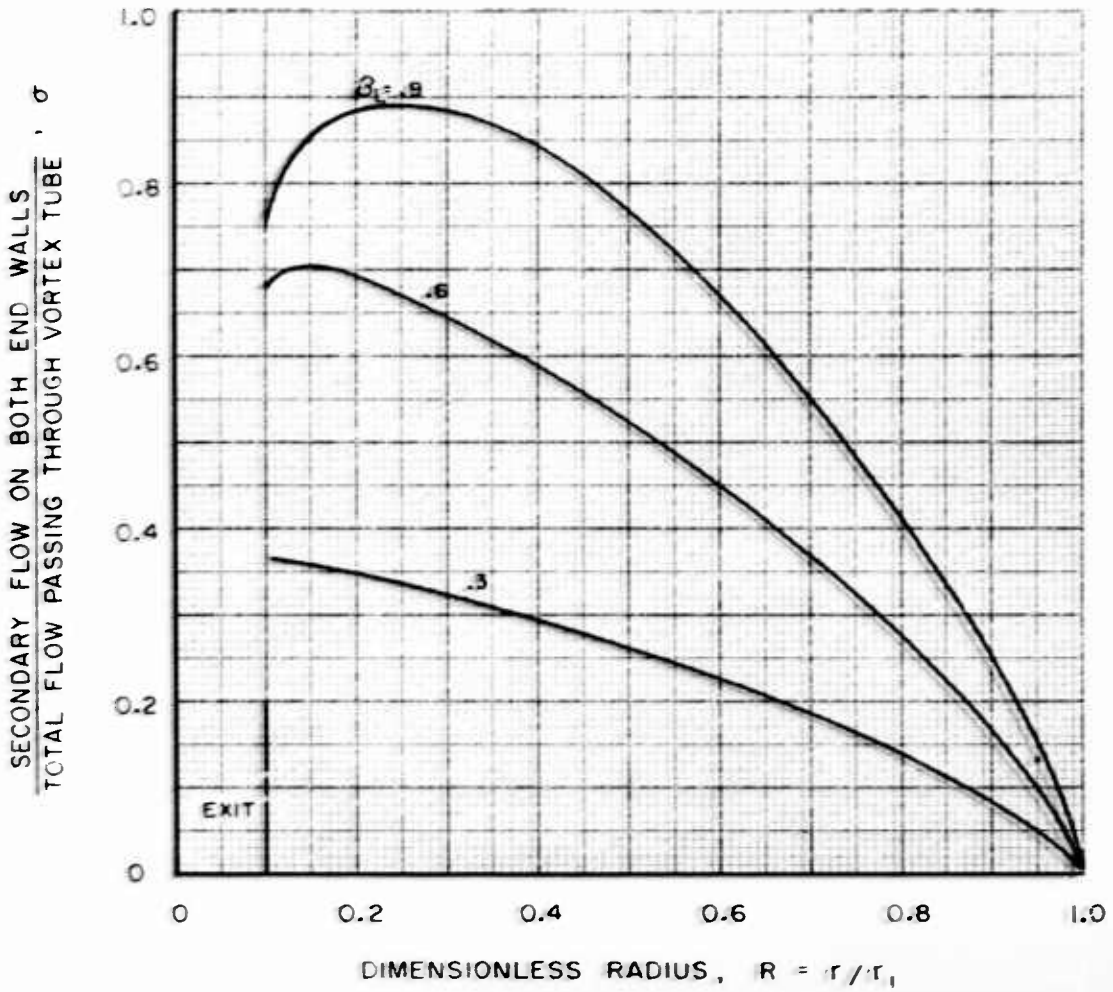

EFFECT OF RADIUS ON BOUNDARY LAYER THICKNESS ON END WALL FOR A RADIAL REYNOLDS NUMBER OF 20

LAMINAR FLOW PROFILES (1) AND (12) IN FIGS 3 AND 4

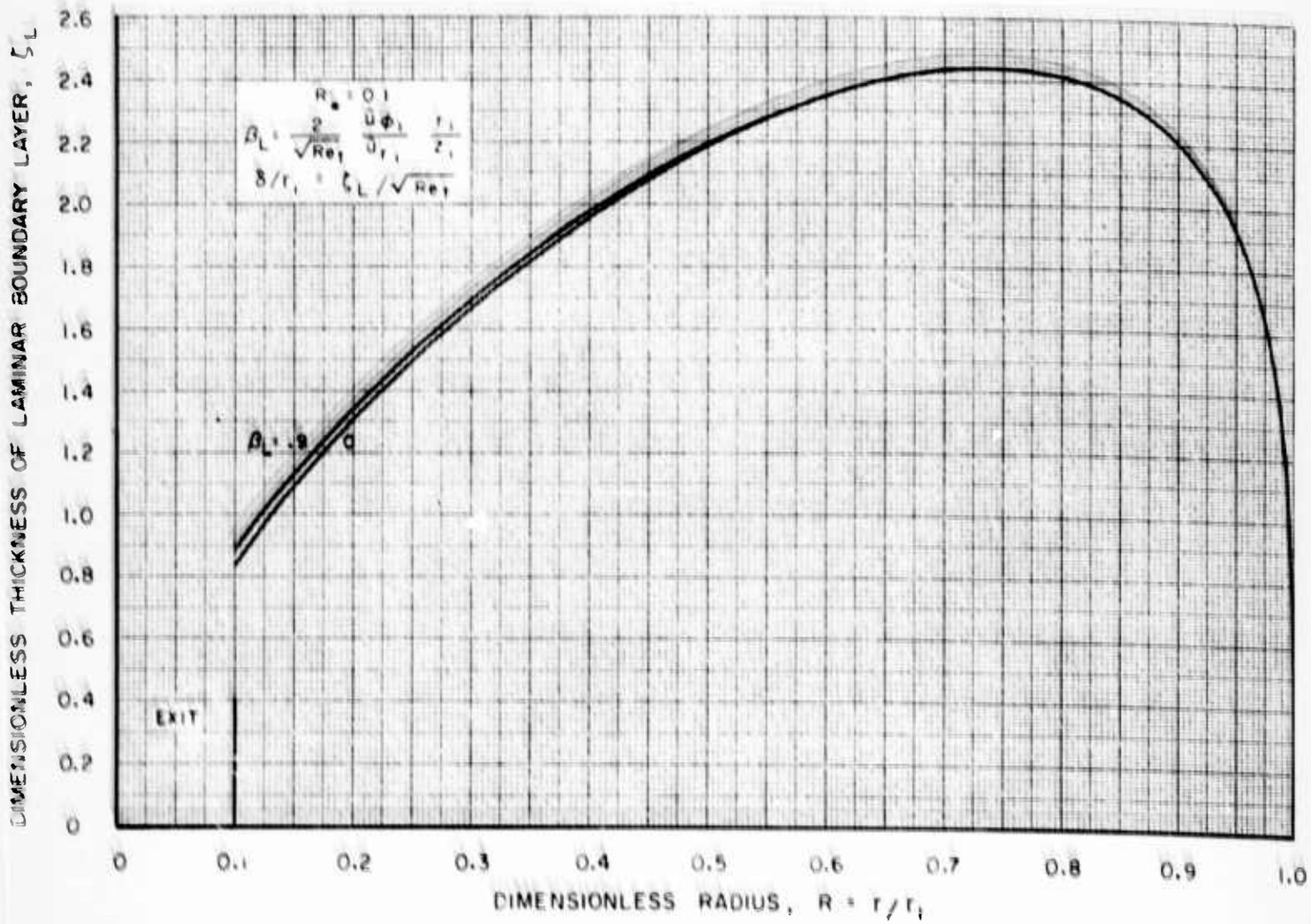

CONFIDENTIAL

FIG. 28

MAXIMUM VALUE OF FRACTION OF TOTAL FLOW WITHIN BOUNDARY LAYERS ON BOTH END WALLS

LAMINAR FLOW PROFILES (1) AND (12) IN FIGS. 3 AND 4

$R_s = 0.1$ $\qquad \beta_L = \frac{2}{\sqrt{Re_1}} \frac{\bar{u}_{\phi_1}}{\bar{u}_{r_1}} \frac{r_1}{z_1} \qquad \sigma_M = \frac{2 W_{s\,MAX}}{2\pi r_1 z_1 \rho \bar{u}_{r_1}}$

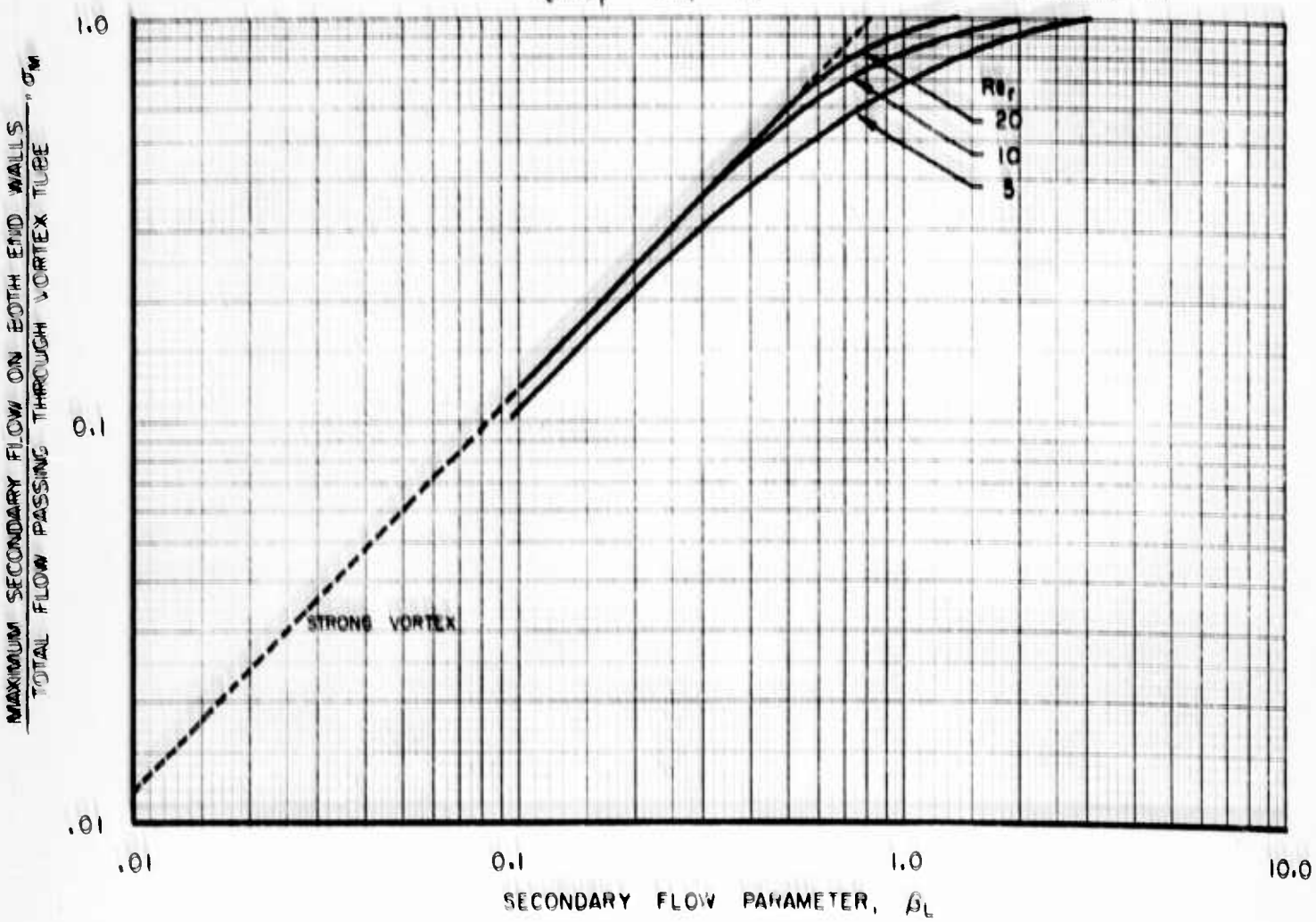

R-2494-11

FIG. 29

CONFIDENTIAL

CONFIDENTIAL

FRACTION OF TOTAL FLOW LEAVING VORTEX TUBE THROUGH END WALL BOUNDARY LAYERS

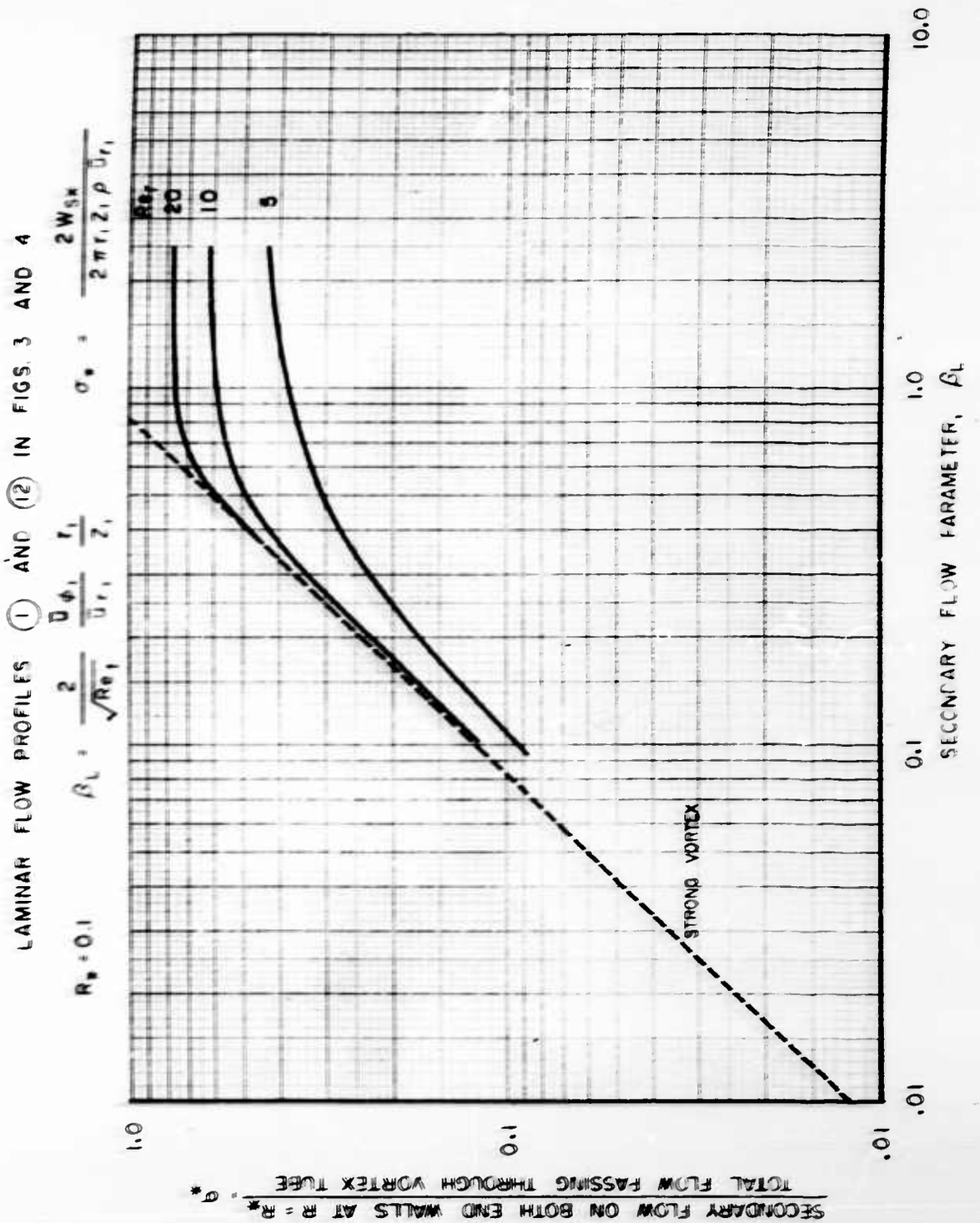

R-2494-1

FRACTION OF TOTAL FLOW PASSING FROM SECONDARY INTO PRIMARY FLOW

FIG. 31

LAMINAR FLOW PROFILES (1) AND (12) IN FIGS. 3 AND 4

$R_* = 0.1$ $\quad \beta_L = \frac{2}{\sqrt{Re_1}} \frac{\bar{u}\phi_1}{\bar{u}_{r_1}} \frac{r_1}{Z_1}$ $\quad \sigma_R = \frac{2W_{SM} - 2W_{S*}}{2\pi r_1 Z_1 \rho \bar{u}_{r_1}}$

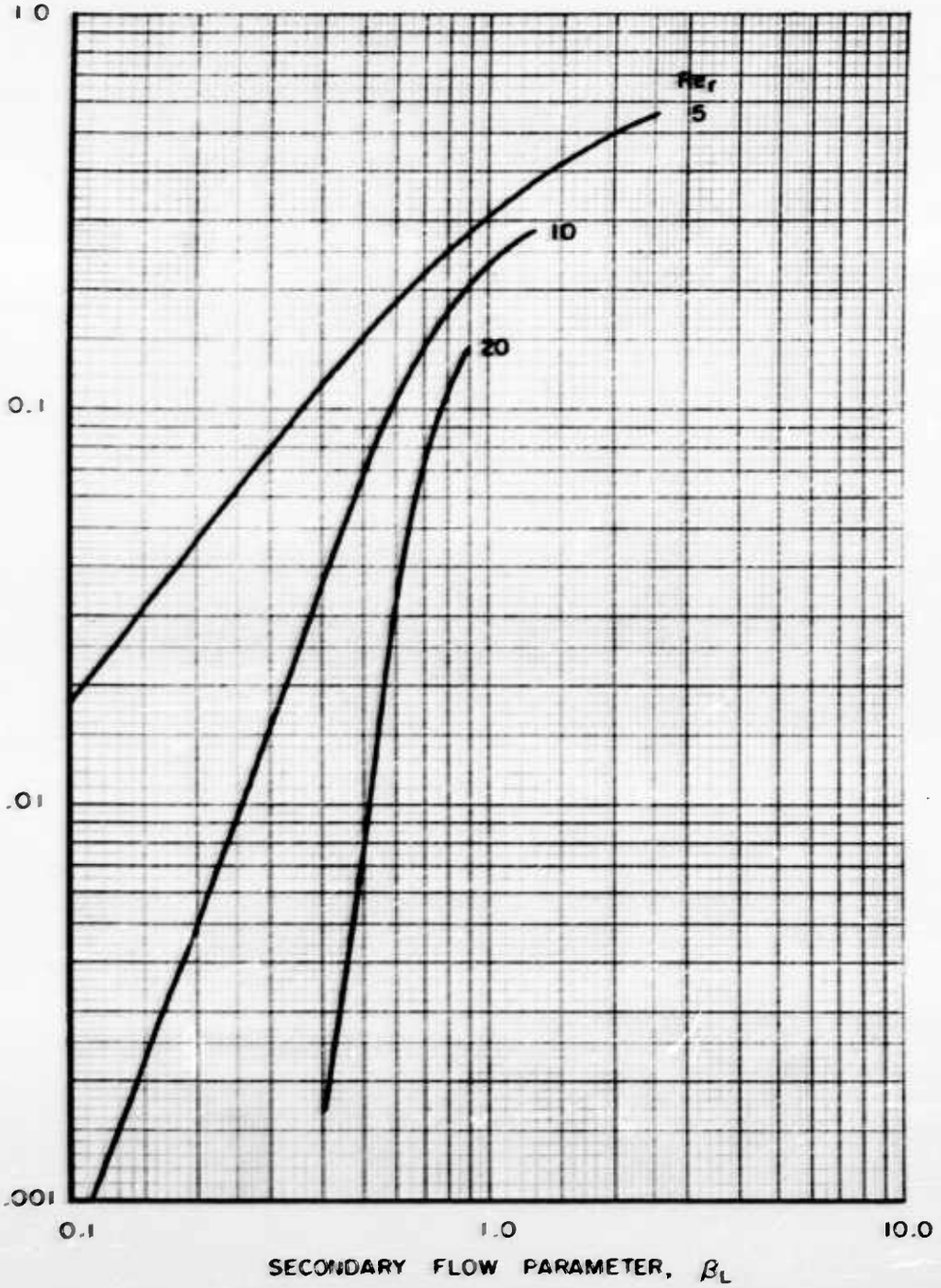

CONFIDENTIAL

FLOW REGIMES IN OPERATION OF A VORTEX TUBE

LAMINAR FLOW PROFILES (1) AND (12) IN FIGS. 3 AND 4

$$\beta_L = \frac{2}{\sqrt{Re_r}} \frac{\bar{u}_{\phi_1}}{\bar{u}_{r_1}} \frac{r_1}{z_1} \qquad Re_r = \frac{r_1 \bar{u}_{r_1}}{\nu}$$

$$\lambda = RU_\phi = \frac{r \bar{u}_\phi}{r_1 \bar{u}_{\phi_1}} \qquad \sigma_M = \frac{2W_{SM}}{2\pi r_1 \rho \bar{u}_{r_1} z_1}$$

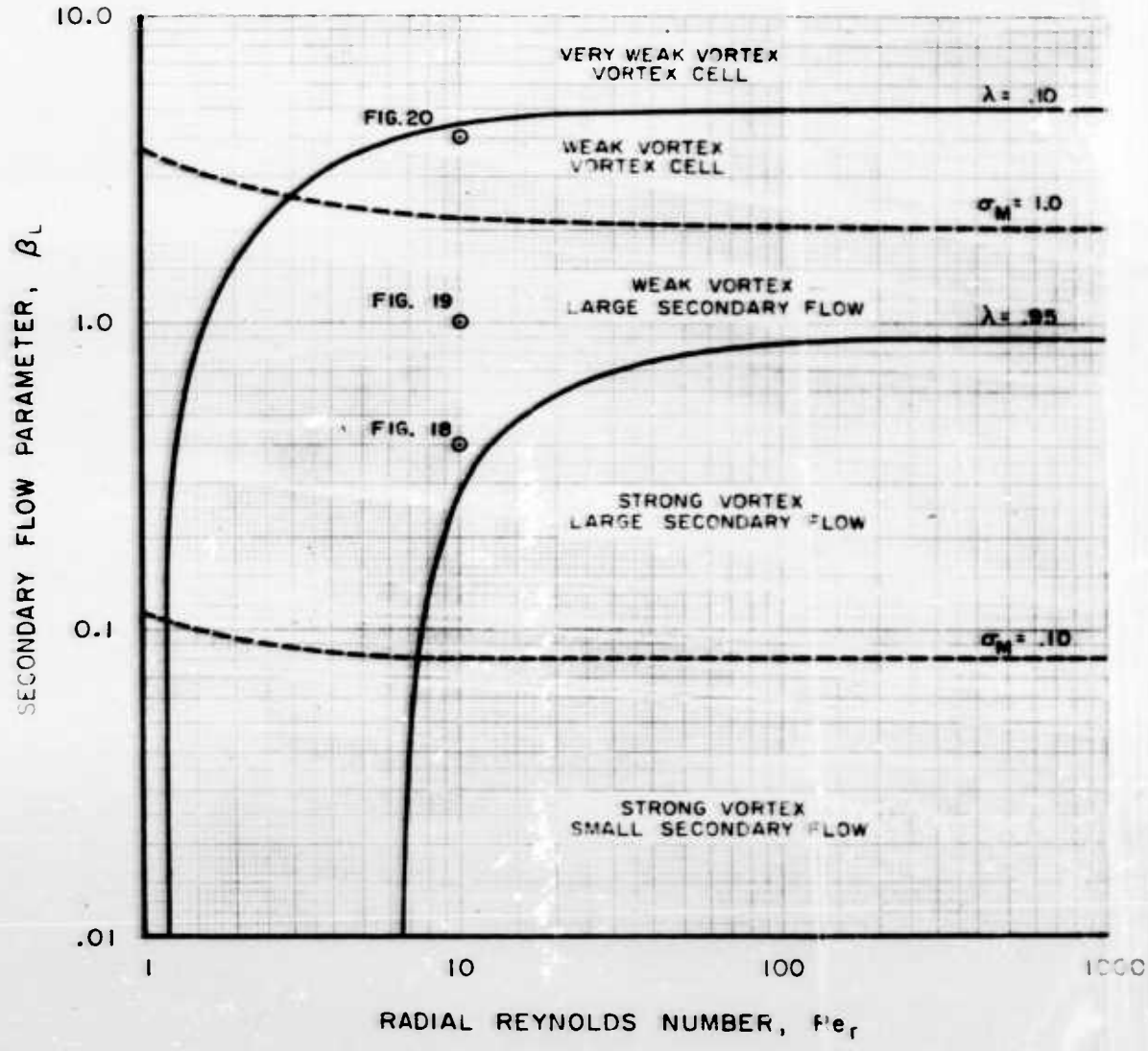

CONFIDENTIAL